THE FASEB JOURNAL • RESEARCH • www.fasebj.org

Osteoblast-derived NOTUM reduces cortical bone mass in mice and the *NOTUM* locus is associated with bone mineral density in humans

Sofia Movérare-Skrtic,[*,1] Karin H. Nilsson,[*,1] Petra Henning,[*] Thomas Funck-Brentano,[*] Maria Nethander,[*] Fernando Rivadeneira,[†] Glaucia Coletto Nunes,[‡] Antti Koskela,[§] Juha Tuukkanen,[§] Jan Tuckermann,[¶] Christine Perret,[‖,#] Pedro Paulo Chaves Souza,[‡,] Ulf H. Lerner,[*,2] and Claes Ohlsson[*,3]**

[*]Department of Internal Medicine and Clinical Nutrition, Institute of Medicine, Centre for Bone and Arthritis Research at the Sahlgrenska Academy, University of Gothenburg, Gothenburg, Sweden; [†]Department of Internal Medicine, Erasmus University Rotterdam, Rotterdam, The Netherlands; [‡]Bone Biology Research Group, School of Dentistry, São Paulo State University (UNESP), Araraquara, Brazil; [§]Department of Anatomy and Cell Biology, Faculty of Medicine, Institute of Cancer Research and Translational Medicine, University of Oulu, Oulu, Finland; [¶]Institute of General Zoology and Endocrinology, University of Ulm, Ulm, Germany; [‖]INSERM, Unité 1016, Institut Cochin, Université Paris Descartes, Sorbonne Paris Cité, Paris, France; [#]Equipe Labellisée Ligue Nationale contre le Cancer, Paris, France; and [**]School of Dentistry, Federal University of Goiás, Goiânia, Brazil

ABSTRACT: Osteoporosis is a common skeletal disease, affecting millions of individuals worldwide. Currently used osteoporosis treatments substantially reduce vertebral fracture risk, whereas nonvertebral fracture risk, mainly caused by reduced cortical bone mass, has only moderately been improved by the osteoporosis drugs used, defining an unmet medical need. Because several wingless-type MMTV integration site family members (WNTs) and modulators of WNT activity are major regulators of bone mass, we hypothesized that NOTUM, a secreted WNT lipase, might modulate bone mass *via* an inhibition of WNT activity. To characterize the possible role of endogenous NOTUM as a physiologic modulator of bone mass, we developed global, cell-specific, and inducible *Notum*-inactivated mouse models. *Notum* expression was high in the cortical bone in mice, and conditional *Notum* inactivation revealed that osteoblast lineage cells are the principal source of NOTUM in the cortical bone. Osteoblast lineage–specific *Notum* inactivation increased cortical bone thickness *via* an increased periosteal circumference. Inducible *Notum* inactivation in adult mice increased cortical bone thickness as a result of increased periosteal bone formation, and silencing of *Notum* expression in cultured osteoblasts enhanced osteoblast differentiation. Large-scale human genetic analyses identified genetic variants mapping to the *NOTUM* locus that are strongly associated with bone mineral density (BMD) as estimated with quantitative ultrasound in the heel. Thus, osteoblast-derived NOTUM is an essential local physiologic regulator of cortical bone mass *via* effects on periosteal bone formation in adult mice, and genetic variants in the *NOTUM* locus are associated with BMD variation in adult humans. Therapies targeting osteoblast-derived NOTUM may prevent nonvertebral fractures.—Movérare-Skrtic, S., Nilsson, K. H., Henning, P., Funck-Brentano, T., Nethander, M., Rivadeneira, F., Coletto Nunes, G., Koskela, A., Tuukkanen, J., Tuckermann, J., Perret, C., Souza, P. P. C., Lerner, U. H., Ohlsson, C. Osteoblast-derived NOTUM reduces cortical bone mass in mice and the *NOTUM* locus is associated with bone mineral density in humans. FASEB J. 33, 11163–11179 (2019). www.fasebj.org

KEY WORDS: osteoporosis · transgenic · WNT16

ABBREVIATIONS: α-MEM, α-minimum essential medium; μCT, micro–computed tomography; ALP, alkaline phosphatase; BMD, bone mineral density; BMM, bone marrow–derived macrophage; BV/TV, bone volume/tissue volume; CT, computed tomography; CTX, C-terminal type I collagen; DXA, dual-energy X-ray absorptiometry; eBMD, estimated bone mineral density; M-CSF, macrophage colony-stimulating factor; PGK-1, phosphoglycerate kinase 1; RANKL, receptor activator of nuclear factor κ-B ligand; siRNA, small interfering RNA; TRAP, tartrate-resistant acid phosphatase; SNP, single nucleotide polymorphism; Wls, Wntless; WNT, Wingless-type MMTV integration site family member; WT, wild type

[1] These authors contributed equally to this work.

[2] Correspondence: Centre for Bone and Arthritis Research, Vita Stråket 11, Sahlgrenska University Hospital, S-413 45 Gothenburg, Sweden. E-mail: ulf.lerner@gu.se

[3] Correspondence: Centre for Bone and Arthritis Research, Vita Stråket 11, Sahlgrenska University Hospital, S-413 45 Gothenburg, Sweden. E-mail: claes.ohlsson@medic.gu.se

doi: 10.1096/fj.201900707R

This article includes supplemental data. Please visit *http://www.fasebj.org* to obtain this information.

Osteoporosis is a common skeletal disease, affecting millions of individuals worldwide, and the prevention of fractures is an important public health goal. Currently, the osteoporosis treatments that are used substantially reduce vertebral fracture risk, whereas nonvertebral fracture risk has only moderately been improved by the osteoporosis drugs used, defining an unmet medical need (1, 2). Although cortical bone mass and composition are major determinants of bone strength and fracture risk in humans (1, 3, 4), only a limited number of studies have focused on the cellular and molecular mechanism specifically regulating cortical bone mass (2). However, it is known that the periosteal surface of the cortical bone is regulated by growth hormone (GH), insulin-like growth factor I (IGF-I), and periostin (5–8).

Wingless-type MMTV integration site family members (WNTs) belong to a family of secreted cysteine-rich glycoproteins that signal *via* either the WNT/β-catenin pathway, also termed the canonical WNT pathway, or the noncanonical WNT pathways. A crucial step for WNT signaling is the interaction between WNTs and their transmembrane receptor proteins frizzled. When WNT proteins are synthesized, an acyl group from palmitoleic acid is attached at a serine amino acid residue (9). This lipid modification of WNT is necessary for its function because the frizzled proteins contain a cleft that specifically interacts with the acyl group. Recent *in vitro* studies have demonstrated that an extracellular enzyme (secreted lipase) called NOTUM renders WNT inactive by specifically removing the acyl group from WNT (9, 10). It has been described that NOTUM is a circulating protein, but the relative importance of circulating *vs.* local NOTUM is unknown (11). In a previous report, lifelong NOTUM inactivation in mice, using the less precise gene trapping technique, resulted in developmental defects involving the kidneys (unilateral agenesis) and teeth (dental dysplasia) as well as reduced embryonic viability (12). Referring to this mouse model of NOTUM inactivation, developed in a large-scale screen of multiple mouse models, it was recently reported that the mice surviving to adulthood had increased cortical bone mass, but the underlying mechanisms for the skeletal phenotype in these mice were not evaluated (13).

Because several WNTs and modulators of WNT activity are major regulators of bone mass (1, 4, 14, 15), we hypothesized that NOTUM might modulate bone mass *via* an inhibition of WNT activity. To characterize the possible role of endogenous NOTUM as a physiologic modulator of bone mass, we developed global, cell-specific, and inducible *Notum*-inactivated mouse models using homologous recombination, allowing precise manipulation of genetic sequences in the mouse. In addition, we determined the cellular and molecular effects of *Notum* using cultured osteoblasts and osteoclasts. Finally, we aimed to determine if genetic variation in the *NOTUM* locus is associated with bone mass in humans.

MATERIALS AND METHODS

Generation of global *Notum*$^{-/-}$ *and Notum*$^{+/-}$ mice

The global *Notum*$^{-/-}$ and *Notum*$^{+/-}$ mice were generated by breeding male *Notum*$^{flox/flox}$ mice (kindly provided by Prof. Christine Perret, INSERM, Institut Cochin) (16), with female mice expressing Cre recombinase ubiquitously and from an early embryonic stage under the control of the phosphoglycerate kinase-1 promoter (PGKcre) (17). In PGKcre-expressing female mice, the Cre activity starts in the diploid phase of oogenesis, and thereby a complete recombination of *LoxP* sites occurs also in *Cre*$^{-}$ offspring. In the *Notum*^{flox} mice, *LoxP* sites are introduced upstream from *Notum* exon 2 and downstream from *Notum* exon 8 and in the presence of an active Cre recombinase, the DNA fragment from exon 2 to exon 8 of the *Notum* gene is excised (16). Presence or absence of the *Notum*^{flox} allele was determined by use of multiplex real-time PCR analysis (StepOnePlus Real-Time PCR System, Thermo Fisher Scientific, Waltham, MA, USA). The following primers and carboxyfluorescein-labeled probe were used for detection of the *Notum*^{flox} allele: forward (5′-CCATGATCCTGTGCCTTTCT-3′), reverse (5′-CGACGCGTGAAGTTCCTATT-3′), and probe (5′-GGCCGCGAAGTTCCTATACT-3′), whereas the following primers and VIC-labeled probe were used for detection of the *Notum*$^{+}$ allele: forward (5′-CCATGATCCTGTGCCTTTCT-3′), reverse (5′-AGTGGCATCGGAGACAAATC-3′), and probe (5′-TTGGCAGCCCCAAAATATAG-3′). Genotyping for the presence of PGKcre was done using forward (5′-AACATGCTTCATCGTCGG-3′) and primer (5′-TTCGGATCATCAGCTACACC-3′).

Briefly, male *Notum*$^{flox/flox}$ mice were bred with PGKcre-expressing female mice generating *Notum*$^{+/-}$ offspring. To generate *Notum*$^{-/-}$, *Notum*$^{+/-}$, and littermate wild-type (WT) control mice for the experiment, *Notum*$^{+/-}$ female and male mice were mated. Male and female mice included in the experiment were euthanized at 15 wk of age.

The degree of *Notum* deletion at the DNA level in different tissues was determined by multiplex real-time PCR analysis using the following primers and carboxyfluorescein-labeled probe: forward (5′-TGGCTTCCCAGCCCATTAAG-3′), reverse (5′-GGCATGCTACAGACAGGTTG-3′), and probe (5′-AGTCTCACCACCCTGCCCTGT-3′). The following primers and VIC-labeled probe were used as a reference because they detect a sequence present in all mice: forward (5′-AGGTCTCAGACGGCAATCAT-3′), reverse (5′-CCTCCACTGCCTGCTAAGAT-3′), and probe (5′-ACCCAGCATGGTGAGGCCTGCC-3′).

Generation of *Runx2cre-Notum*$^{flox/flox}$ mice

To generate specific inactivation of *Notum* in the osteoblast lineage, *Notum*$^{flox/flox}$ mice were bred with the previously described *Runx2-cre* mice (2, 18). These *Runx2-creNotum*$^{flox/flox}$ mice display early osteoblast-specific *Cre* expression and have the capacity to recombine *LoxP*-flanked DNA sequences in an early osteoblast-specific manner, and an efficient recombination occurs at all sites of endochondral and intramembranous bone formation (particularly in periosteal cells, osteoblasts, and osteocytes but not osteoclasts) when *Runx2-cre* mice were crossed to a Rosa26 reporter strain (18). To generate mice depleted of *Notum* in osteoblasts, female mice with 2 floxed *Notum* alleles (*Notum*$^{flox/flox}$) were mated with male mice having 1 floxed *Notum* allele and 1 allele of *Runx2-cre* (*Runx2-creNotum*$^{+/flox}$). The littermate control mice were *Notum*$^{flox/flox}$. *Runx2-cre* mice have an unchanged skeletal phenotype compared to WT mice (2). Genotyping of *Notum*^{flox} mice was performed as described above, whereas the presence of the *Runx2-cre* gene was determined using a 3-primer strategy. The common 5′ primer (5′-CCAGGAAGACTGCAAGAAGG-3′) binds to the *Runx2* promoter of the endogenous gene and the transgene. The 3′ primer (5′-TGGCTTGCAGGTACAGGAG-3′) binds to the *Cre* sequence, and another 3′ primer (5′-GGAGCTGCCGAGTCAATAAC-3′) binds to the endogenous *Runx2*. Male and female *Runx2-creNotum*$^{flox/flox}$ mice included in the experiment were euthanized at 17 wk of age.

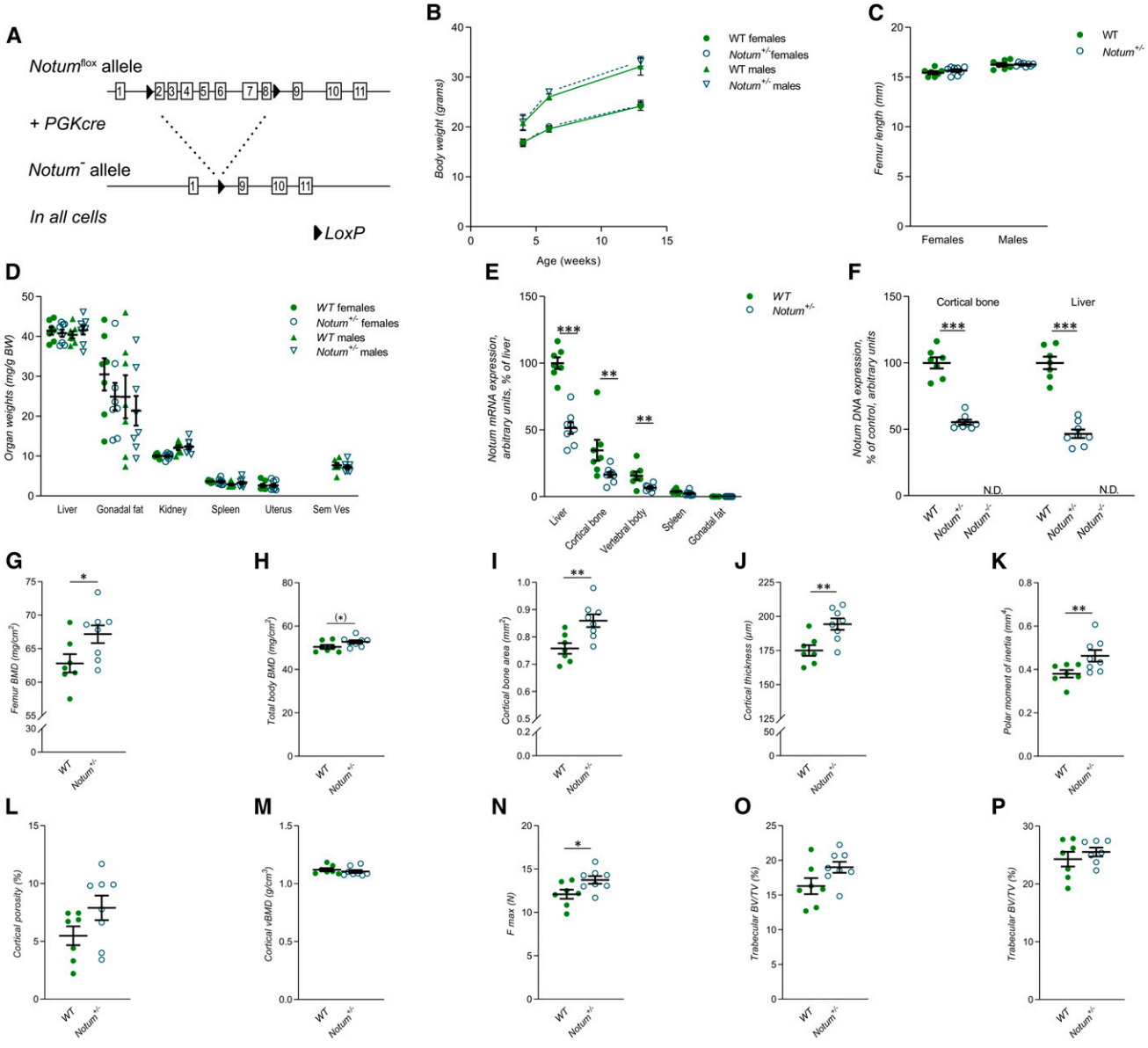

Figure 1. Heterozygous female *Notum*-inactivated mice have increased cortical bone thickness. *A*) Schematic drawing of the global *Notum*-inactivated mouse model. *B*) Normal body weight in both male and female $Notum^{+/-}$ mice ($n = 8$) when comparing with WT mice ($n = 7$) at 4, 6, and 13 wk of age. *C*) $Notum^{+/-}$ mice ($n = 8$) have normal femur length compared to WT mice ($n = 7$). *D*) Soft tissue weights over body weight in male and female $Notum^{+/-}$ ($n = 8$) and WT ($n = 7$) mice. *E*) mRNA expression analyses of *Notum* in liver, cortical bone, vertebral body, spleen, and gonadal fat, as normalized to WT liver, in male $Notum^{+/-}$ ($n = 8$) and WT ($n = 7$) mice. *F*) Degree of deletion in purified DNA from male WT ($n = 7$), $Notum^{+/-}$ ($n = 8$), and $Notum^{-/-}$ ($n = 2$) mice in cortical bone and liver. *G*, *H*) Femur BMD (females, *G*) and total body BMD (*H*) as measured by DXA in $Notum^{+/-}$ (female, $n = 8$) and WT mice (female, $n = 7$). *I*–*M*) Cortical bone area (*I*), cortical thickness (*J*), mean polar moment of inertia (*K*), cortical porosity (*L*), and cortical volumetric BMD (*M*) of the femur as measured by µCT in female $Notum^{+/-}$ ($n = 8$) and WT ($n = 7$) mice. *N*) Maximal load (F max) of the humerus as measured by 3-point bending analyses in female $Notum^{+/-}$ ($n = 8$) and WT ($n = 7$) mice. *O*, *P*) Trabecular bone volume/tissue volume (BV/TV) of the femur (*O*) and of the vertebrae L5 (*P*) as measured by µCT in female $Notum^{+/-}$ ($n = 8$) and WT ($n = 7$) mice. Unless otherwise stated, the results refer to 13-wk-old mice. N.D., not detectable; Sem Ves, seminal vesicles. All values are given as means ± SEM. (*) $P = 0.09$, * $P < 0.05$, ** $P < 0.01$, *** $P < 0.001$ *vs.* WT mice (Student's *t* test).

Generation of mice with inducible *Notum* inactivation

In order to study the acute adult effects of *Notum*, avoiding confounding developmental effects, inducible *Notum* knockout mice were created by breeding the $Notum^{flox/flox}$ mice with the previously described B6.Cg-Tg(CAG-Cre/Esr1*)5Amc/J (CAGGCre-ER, 004682; The Jackson Laboratory, Bar Harbor, ME, USA) transgenic mice (19). Briefly, a male transgenic mouse expressing a tamoxifen-inducible Cre-mediated recombinase, and a $Notum^{+/flox}$ allele (hereafter called *CAGGCre-ER-*$Notum^{+/flox}$) were bred with female $Notum^{flox/flox}$ mice, creating *CAGGCre-ER-*$Notum^{flox/flox}$ mice. $Notum^{flox/flox}$ littermates were used as controls. Genotyping of the $Notum^{flox/flox}$ mice was done as previously described, and the presence of the Cre construct was determined using the following primers: Cre forward:

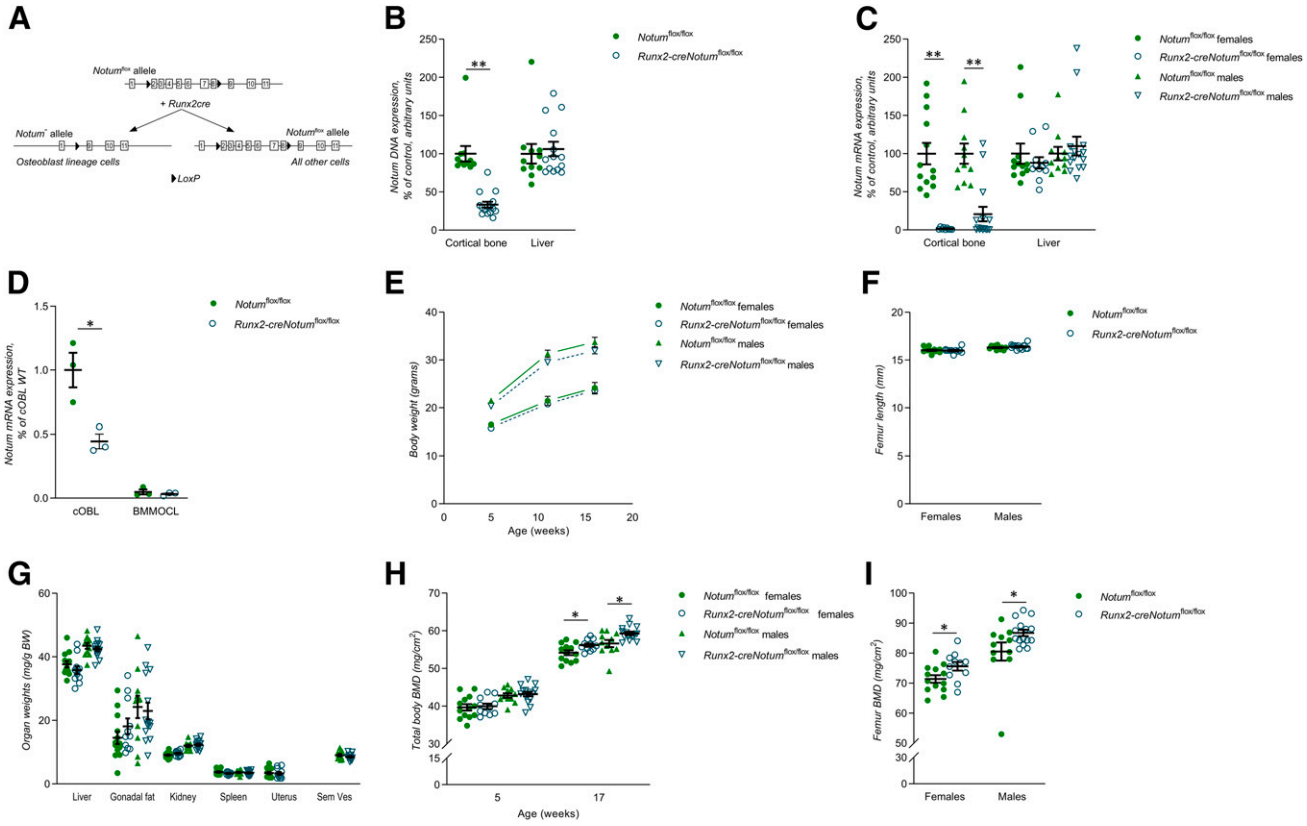

Figure 2. Osteoblast-derived NOTUM is the principal source of NOTUM in bone. *A*) Schematic drawing of the conditional osteoblast lineage–specific *Notum*-inactivated mouse model. *B*) Degree of deletion of *Notum* DNA in cortical bone and liver in *Runx2-creNotum*$^{flox/flox}$ ($n = 15$) and *Notum*$^{flox/flox}$ ($n = 11$) male mice. *C*) mRNA expression analyses of *Notum* in the cortical bone and liver in *Runx2-creNotum*$^{flox/flox}$ (females, $n = 11$; males, $n = 15$) and *Notum*$^{flox/flox}$ (females, $n = 13$; males, $n = 11$) mice. *D*) mRNA expression analyses of *Notum* in cultured calvarial osteoblasts (cOBL) and bone marrow macrophage–derived osteoclasts (BMMOCLs) from *Runx2-creNotum*$^{flox/flox}$ and *Notum*$^{flox/flox}$ mice. (Representative experiment, $n = 3$ wells/cell type and mouse strain.) *E*) Normal body weight in *Runx2-creNotum*$^{flox/flox}$ mice (female, $n = 11$; male, $n = 15$) compared to *Notum*$^{flox/flox}$ mice (female, $n = 13$; male, $n = 11$) at 5, 12, and 17 wk of age. *F*) Normal femur length in *Runx2-creNotum*$^{flox/flox}$ mice (female, $n = 11$; male, $n = 15$) compared to *Notum*$^{flox/flox}$ mice (female, $n = 13$; male, $n = 11$). *G*) Soft tissue weights over body weight in *Runx2-creNotum*$^{flox/flox}$ mice (females, $n = 11$; males, $n = 15$) and *Notum*$^{flox/flox}$ mice (females, $n = 13$; males, $n = 11$). *H*) Total body BMD as measured by DXA in 5-wk-old and 17-wk-old *Runx2-creNotum*$^{flox/flox}$ mice (female, $n = 11$; male, $n = 15$) and *Notum*$^{flox/flox}$ mice (female, $n = 13$; male, $n = 11$). *I*) Femur BMD as measured by DXA in 17-wk-old *Runx2-creNotum*$^{flox/flox}$ mice (female, $n = 11$; male, $n = 15$) and *Notum*$^{flox/flox}$ mice (female, $n = 13$; male, $n = 11$). Unless otherwise stated, the results refer to 17-wk-old mice. All values are given as means ± SEM. $^*P < 0.05$, $^{**}P < 0.01$ *vs.* *Notum*$^{flox/flox}$ mice (Student's *t* test).

5′-GCGGTCTGGCAGTAAAAACTATC-3′; Cre reverse: 5′-GTGAAACAGCATTGCTGTCACTT-3′; WT forward: 5′-CTAGGCCACAGAATTGAAAGATCT-3′; and WT reverse: 5′-GTAGGTGGAAATTCTAGCATCATCC-3′.

To study the adult effects of NOTUM on cortical bone thickness and bone strength, avoiding confounding developmental effects, a long-term study using female *CAGGCre-ER-Notum*$^{flox/flox}$ mice was performed. Female 11-wk-old *CAGGCre-ER-Notum*$^{flox/flox}$ and *Notum*$^{flox/flox}$ littermate control mice were injected with tamoxifen (50 mg/kg; T5648; MilliporeSigma, Burlington, MA, USA) for 3 consecutive days to activate the Cre construct. The mice were euthanized 31 d after the first tamoxifen injection at the age of 15 wk. To mechanistically study the importance of NOTUM in a short-term study, 20-wk-old male *CAGGCre-ER-Notum*$^{flox/flox}$ and *Notum*$^{flox/flox}$ littermate control mice were injected with tamoxifen for 3 consecutive days. The mice were euthanized 11 d after the first tamoxifen injection at the age of 22 wk.

The experimental procedures involving animals were approved by the Ethics Committee at the University of Gothenburg, and the care of the animals was in accordance with its guidelines. The mice were housed in a standard animal housing facility with 12-h dark/light periods. The temperature was controlled (22°C), and food and water were available *ad libitum*. At termination, the animals were anesthetized with Ketador/Dexdomitor (Richter Pharma, Wels, Austria/Orion Oyj, Espoo, Finland), bled, and euthanized by cervical dislocation. Long bones and vertebrae were dissected and stored for future analyses, and soft tissues were collected, weighed, and snap-frozen in liquid nitrogen.

Assessment of murine bone parameters

Dual-energy X-ray absorptiometry

Total body and femur bone mineral density (BMD) were assessed using Lunar PIXImus densitometer (Wipro GE Healthcare, Chicago, IL, USA), or the UltraFocus^{DXA} (Faxitron Bioptics, Tucson, AZ, USA) (2, 20).

High-resolution micro–computed tomography

High-resolution micro–computed tomography (μCT) was used to analyze distal femur, proximal tibia, and vertebrae L5 (Skyscan

TABLE 1. *Increased cortical bone mass in mice with inducible* Notum *inactivation*

Variable	*Notum*$^{flox/flox}$	*CAGG-Cre-ER-Notum*$^{flox/flox}$
DXA		
Femur BMD (mg/cm^2)	104.2 ± 1.8	109.2 ± 1.5*
Total body BMD (mg/cm^2)	73.2 ± 0.8	75.4 ± 0.7$^{\#}$
CT (tibia)		
Cortical bone area (mm^2)	0.87 ± 0.02	0.93 ± 0.02*
Cortical bone thickness (μm)	222 ± 5	234 ± 3*
Mean polar moment of inertia (mm^4)	0.33 ± 0.01	0.37 ± 0.02*
Cortical porosity (%)	6.4 ± 0.8	5.8 ± 0.6
Cortical volumetric BMD (g/cm^3)	1.22 ± 0.02	1.23 ± 0.02
Trabecular bone volume/tissue volume (%)	20.1 ± 1.5	21.6 ± 0.7

Values are given as means ± SEM. (*Notum*$^{flox/flox}$, $n = 10$; *CAGG-Cre-ER-Notum*$^{flox/flox}$, $n = 12$; 15-wk-old female mice; $^{\#}P = 0.056$). $*P < 0.05$ *vs.* *Notum*$^{flox/flox}$ (Student's *t* test).

1172; Bruker MicroCT, Aartselaar, Belgium) (2). The cortical region was analyzed in the diaphyseal region of femur and tibia, starting at a distance of ≈5.2 mm from the growth plate and continuing a further 134 μm in proximal direction for femur and in the distal direction for tibia. Trabecular bone was analyzed in the metaphyseal region of the femur and tibia, starting ≈650 μm from the growth plate and continuing a further 134 μm in proximal direction for femur and in distal direction for tibia. In the L5 vertebral body, the trabecular bone caudal of the pedicles was selected for analysis commencing at a distance of approx. 4.5 μm caudal of the lower end of the pedicles, and extending a further longitudinal distance of 230 μm in the caudal direction. Within the trabecular region, the trabecular bone was manually separated from the cortical bone by contouring the irregular anatomic structure adjacent to the endocortical boundary on a slice-by-slice basis. The grayscale μCT images were processed by a global threshold segmentation using the CTAn software (Bruker MicroCT) (2).

Peripheral quantitative computed tomography

Computed tomography (CT) scans were performed using the peripheral quantitative computed tomography XCT Research M (v.4.5B; Norland Stratec, Pforzheim, Germany) with a voxel size of 70 μm, as previously described by Windahl *et al.* (21). To measure trabecular volumetric BMD, the scan was positioned in the metaphysis of the femur at a distance corresponding to 3.4% of the total femur length, proximal from the distal growth plate. This area contained trabecular and cortical bone, and the trabecular region was therefore defined as the inner 45% of the total cross-sectional area. The cortical bone parameters were analyzed in the middiaphyseal region of the femur, which is an area that contains only cortical bone. The threshold for cortical bone was set to 710 mg/cm^3 (22).

Mechanical strength

After dissection, the humerus was frozen at −20°C. Three-point bending was performed with a span length of 4.5 mm and a loading speed of 0.155 mm/s using an Instron 3366 (Instron, Norwood, MA, USA). Biomechanical parameters, based on the recorded load deformation curves, were calculated from Bluehill 2 software v.2.6 (Instron) with custom-made Excel (Microsoft, Redmond, WA, USA) macros (2).

Bone histomorphometry

For dynamic histomorphometry, the mice were intraperitoneally injected with the fluorochromes calcein and alizarin (Merck GmbH, Darmstadt, Germany) 9 and 2 d prior to termination, respectively (2). Upon dissection, femur and tibia were fixated in 4% formaldehyde, dehydrated in 70% EtOH, and imbedded in methyl methacrylate. The femur and tibia were cut in 200-μm-thick transverse cross-sectional sections in the middiaphyseal region (for dynamic cortical histomorphometry), as well as in 4-μm-thick longitudinally coronary sections (for static histomorphometry). The analyses of dynamic cortical bone

TABLE 2. *Increased number of periosteal osteoblasts in mice with inducible* Notum *inactivation*

Variable	*Notum*$^{flox/flox}$	*CAGG-Cre-ER-Notum*$^{flox/flox}$
Periosteal		
Number of osteoblasts/perimeter (mm^{-1})	1.9 ± 0.6	5.6 ± 1.3*
Osteoblast surface/bone surface (%)	4.0 ± 1.3	11.5 ± 2.7*
Number of osteoclasts/perimeter (mm^{-1})	0.8 ± 0.1	0.9 ± 0.1
Osteoclast surface/bone surface (%)	2.7 ± 0.4	2.7 ± 0.4
Endocortical		
Number of osteoblasts/perimeter (mm^{-1})	23.3 ± 2.7	18.0 ± 2.1
Osteoblast surface/bone surface (%)	46.4 ± 5.8	34.5 ± 4.1
Number of osteoclasts/perimeter (mm^{-1})	1.3 ± 0.2	1.2 ± 0.2
Osteoclast surface/bone surface (%)	4.1 ± 0.7	3.4 ± 0.5

Values are given as means ± SEM. (*Notum*$^{flox/flox}$, $n = 12$; *CAGG-Cre-ER-Notum*$^{flox/flox}$, $n = 10$; 22-wk-old male mice). $*P < 0.05$ *vs.* *Notum*$^{flox/flox}$ (Student's *t* test).

parameters were performed without any staining. For analyses of cellular parameters, the 4-μm-thick sections were stained with Masson-Goldner trichrome. Osteoclasts were defined in Masson-Goldner trichrome–stained sections as bone-resorbing multinucleated cells (2 or more nuclei) in contact with cortical bone surface. The bone-resorbing nature was identified using the shape of the cell (compared to other endosteal cells, including flat mononuclear bone lining cells and cuboidal mononuclear osteoblasts) and the possible presence of eroded surface (23, 24). All parameters were measured using the OsteoMeasure Histomorphometry Analysis System software v.2.2 (Osteometrics, Atlanta, GA, USA), following the guidelines of the American Society for Bone and Mineral Research (25).

Measurement of serum markers

To assess bone resorption, serum levels of C-terminal type I collagen (CTX) fragments were measured using an ELISA RatLaps Kit (Immunodiagnostic Systems, East Boldon, United Kingdom). Serum levels of procollagen type I N-terminal propeptide were measured using a Rat/Mouse EIA Kit (Immunodiagnostic Systems) as a marker of bone formation.

Cell cultures

Silencing of Notum in MC3T3-E1 osteoblasts

Gene expression analyses in primary calvarial cell cultures from WT mice showed that expression of *Notum* mRNA was down-regulated during culture to an expression level similar to that in cells from *Runx2-creNotum*$^{flox/flox}$ mice (Supplemental Fig. S1*A*). The mRNA expression of *Notum* was also decreased in primary cultures of osteoblasts from long bones (Supplemental Fig. S1*B*). This finding, together with the fact that these cells are a mixture of *Runx2*-expressing cells and other cell types present in the bones used for isolation, made us select the murine preosteoblastic cell line MC3T3-E1 for studies on the role of endogenous NOTUM in osteoblast differentiation. An important observation for this selection was the finding that the *Notum* mRNA expression in the MC3T3-E1 cells was not decreased in cell cultures over 11 d (Supplemental Fig. S2), in contrast to primary bone cell cultures.

MC3T3-E1 (CRL-2593, subclone 4; American Type Culture Collection, Manassas, VA, USA) was maintained in α-minimum essential medium (α-MEM, M0450; Thermo Fisher Scientific; MilliporeSigma) supplemented with 10% heat inactivated fetal bovine serum (16000-044; Thermo Fisher Scientific), 2 mM L-glutamine, 100 U/ml penicillin, and 100 μg/ml streptomycin. For experiments, cells were seeded at an initial density of 10,000 cells in 500 μl of culture medium in 48-well culture dishes (Corning, Corning, NY, USA). To induce osteogenic differentiation, osteogenic medium was prepared by further supplementation with 50 μg/ml L-ascorbic acid and 4 mM β-glycerophosphate (MilliporeSigma). Medium was replaced every 2 d for the duration of all experiments. All cells were maintained at 37°C in a humidified 5% CO_2 environment.

To assess the role of NOTUM in osteoblast differentiation, *Notum* mRNA was silenced using a specific small interfering RNA (siRNA) sequence (Invitrogen Silencer Predesigned siRNA 4390771, S95064; Thermo Fisher Scientific). A scrambled sequence (AM4635) was used as negative control. Twenty-four and 72 h after seeding, the cells were transfected with 30 nM of the siRNA using lipofectamine RNAiMax (Thermo Fisher Scientific) in serum-free OptiMEM (Thermo Fisher Scientific). Cells were harvested 24 h after the first and second transfection for gene expression analyses. For quantification of alkaline phosphatase (ALP) activity and ALP staining, cells were exposed to osteogenic media 24 h after the second silencing, with an additional silencing 3 d later. Seven days after exposure to osteogenic media, cells were stained for ALP and enzyme activity was analyzed quantitatively.

ALP analyses

At the end of osteogenic treatment, the cells were fixed with 70% ethanol for 10 min and stained for ALPase activity using a commercial kit (86R; MilliporeSigma) following the manufacturer's instructions and photographed. For quantification of ALPase activity, proteins from another plate were extracted using 200 μl of ultrapure water and exposed to 5 thermal shock cycles for 20 min at −20°C and 15 min at 37°C. Proteins were quantified using Bicinchoninic Acid Assay Kit (23235; Thermo Fisher Scientific). For ALPase activity measurement, a commercial kit based on the ability of ALP to hydrolyze thymolphthalein monophosphate releasing thymolphthalein was used (Labtest Diagnostica, Lagoa Santa, Brazil). Briefly, 10 μg of proteins were used in a final volume of 80 μl of the reaction buffer (pH 10.1) containing 2.75 mM of thymolphthalein monophosphate and incubated at 37°C for 90 min in a 96-well ELISA plate (Corning). After the reaction period, 200 μl of color reagent was added to each well and the absorbance was measured at 580 nM using a spectrophotometer (Epoch; Biotek, Winooski, VT, USA).

Primary bone cell cultures

Primary calvarial periosteal bone cells from 3- to 5-d-old C57BL/6N *Notum*$^{flox/flox}$ and *Runx2-creNotum*$^{flox/flox}$ mice were isolated by sequential enzymatic digestion as previously described in refs. 26 and 27. Isolated periosteal bone cells were cultured in complete α-MEM (22561-021; Thermo Fisher Scientific) supplemented with 10% heat inactivated fetal bovine serum (F7524; MilliporeSigma), 2 mM GlutaMax (35050-038; Thermo Fisher Scientific), 50 μg/ml gentamicin (15750-037; Thermo Fisher Scientific), 100 U/ml penicillin and 100 μg/ml streptomycin (15140-148; Thermo Fisher Scientific) for 3–5 d prior to experiment start. At the start of the experiment, cells were seeded at 20,000 cells/cm^2 in 48 well plates and incubated in osteogenic media [complete α-MEM supplemented with 10 mM β-glycerophosphate disodium salt hydrate (BGP, G9422; MilliporeSigma) and 0.2 mM L-ascorbic acid 2-phosphate sesquimagnesium salt hydrate (Asc-2P, A8960; MilliporeSigma)]. Culture media were replenished after 4 d and cells were harvested for RNA analysis after 4 and 7 d of culture. Primary bone cell cultures from femur and tibia from 8- to 12-wk-old C57BL/6N mice were isolated by outgrowth of cells from collagenase-treated diaphyseal cortical bone as previously described by Bakker and Klein-Nulend (27). Primary bone cells from femur and tibia were isolated in complete α-MEM, and thereafter experiments were performed in osteogenic medium as for calvarial bone cells above.

Primary osteoclast cell cultures

Bone marrow cells from 8- to 12-wk-old *Notum*$^{flox/flox}$ and *Runx2-creNotum*$^{flox/flox}$ mice were cultured in suspension culture discs (Corning) in complete α-MEM with 30 ng/ml macrophage colony-stimulating factor (M-CSF) (416-ML-050; R&D Systems, Minneapolis, MN, USA) for 2 d, and the adherent bone marrow–derived macrophages (BMMs) were used as osteoclast progenitors (28, 29). BMMs were detached and spot seeded in 24-well plates (40,000 cells/well) and cultured in complete α-MEM with 30 ng/ml M-CSF with or without the addition of 4 ng/ml receptor activator of nuclear factor κ-B ligand (RANKL) (462-TEC; R&D Systems) to induce osteoclast differentiation. The medium was changed after 3 d and cells harvested for RNA isolation by lysis in RLT buffer (Qiagen, Germantown, MD, USA) 4 d after seeding.

Treatment of osteoclasts with recombinant NOTUM

Osteoclasts were differentiated from BMMs as described above. Cells were cultured in M-CSF and RANKL with or without the addition of 10 or 100 ng/ml recombinant human NOTUM (9118-NM; R&D Systems) for 3–4 d before staining for expression of tartrate-resistant acid phosphatase (TRAP) using a commercial staining kit (387A; MilliporeSigma) or lysis in RLT buffer for RNA purification. To study osteoclast formation and activity on bone, 20,000 BMMs were seeded on bovine bone discs (IDS Nordic, Copenhagen, Denmark) in 96-well plates. Media were changed and saved for analysis every 3–4 d, and staining for TRAP was performed after 10 d. The total amount of TRAP5b in the culture media were analyzed as a measure of osteoclastogenesis using a commercial kit (IDS Nordic). Resorptive activity, as assessed by the release of C-terminal telopeptides of type I collagen (CTX-I) from the bone slices, was measured using commercial CTX ELISA (IDS Nordic).

Lipase activity measurement of recombinant NOTUM

Functional enzyme activity of recombinant human NOTUM was tested using the fluorogenic substrate 8-Octanoyloxypyrene-1-3-6-trisulfonic acid trisodium salt (74875; MilliporeSigma). Recombinant NOTUM (50 ng) dissolved in 0.1% bovine serum albumin in PBS (25 μl) was mixed with an equal volume of 5 mM 8-Octanoyloxypyrene-1-3-6-trisulfonic acid trisodium salt in 2 times reaction buffer (10 mM $CaCl_2$, 1 mM $MgCl_2$, 50 mM TrisHCl, pH 7.4). Fluorescence intensity at 535 nm was measured after 10, 20, and 30 min using a SpectraMax i3 (Molecular Devices, Sunnyvale, CA, USA). Wheat germ lipase (L3001, 250 ng; MilliporeSigma) was used as positive control and 0.1% bovine serum albumin in PBS was used as blank.

Real-time quantitative PCR

Total mRNA was prepared from bone using Trizol reagent (15596018; Thermo Fisher Scientific) and RNeasy Mini Kit (74106; Qiagen). For preparation of total mRNA from cultured cells, the RNeasy Micro Kit (74004; Qiagen) or Total RNA Purification Kit (DPK-108L; Cellco, Basking Ridge, NJ, USA) were used. The mRNA was reversed transcribed into cDNA (4368814; Thermo Fisher Scientific), and real-time PCR analyses were performed using the StepOnePlus Real-Time PCR System (Thermo Fisher Scientific) and Assay-on-Demand primer and probe sets (*Notum*: Mm01253273_m1, *Alpl*: Mm00475834_m1, *Acp5 (Trap)*: Mm00475698_m1, *Nfatc1:* Mm00479445_m1, *Ctsk:* Mm00484036_m1; Thermo Fisher Scientific). The expression of each gene was adjusted to 18S ribosomal subunit (4310893E; Thermo Fisher Scientific) or *Actb* custom-made primers: forward (5′-GGACCTGACGGACTACCTCATG-3′), reverse (5′-TCTTTGATGTCACGCACGATTT-3′), used as an internal standard.

All assays had 90–100% efficiency, thus the $2^{-\Delta\Delta Ct}$ method was used to calculate the relative gene expression.

Statistical analyses

Values are given as means ± SEM. The statistical difference between *Runx2-creNotum*$^{flox/flox}$ mice and *Notum*$^{flox/flox}$ mice, between *CAGGCre-ER-Notum*$^{flox/flox}$ and *Notum*$^{flox/flox}$ mice, as well as between *Notum*$^{+/-}$ mice and WT mice, were calculated using an unpaired, 2-tailed Student's *t* test. Statistical differences between cell culture treatment groups were calculated using an unpaired, 2-tailed Student's *t* test when there were 2 groups (cells from 2 mouse strains or 2 treatment groups) and using 1-way ANOVA and Tukey's multiple comparison test when there were more than 2 treatment groups. A difference was considered statistically significant if $P < 0.05$.

Large-scale human genetic analyses using the UK Biobank

In 2006–2010, the UK Biobank recruited 502,647 individuals aged 37–76 yr from across the United Kingdom. All participants provided information regarding their health and lifestyle *via* touch screen questionnaires, consented to physical measurements, and agreed to have their health followed. They also provided blood for future analysis. UK Biobank has ethical approval from the Northwest Multicenter Research Ethics Committee, and informed consent was obtained from all participants.

Estimated BMD using ultrasound

Quantitative ultrasound of the heel was used to obtain a noninvasive estimate of BMD that predicts fracture (30, 31). A Sahara Clinical Bone Sonometer (Hologic, Marlborough, MA, USA) was used for quantitative ultrasound assessment of calcanei in UK Biobank participants. Details of the complete protocol are publicly available on the UK Biobank website (*https://www.ukbiobank.ac.uk/*). Estimated BMD (eBMD; g/cm^2) was derived as a linear combination of speed of sound (SOS in the following equation) and bone ultrasound attenuation (BUA in the following equation) [eBMD = 0.0025926 × (BUA + SOS) − 3.687] (31).

Genotyping

Genotype data are available for ≈488,000 participants in the UK Biobank cohort. Genotyping was performed using the Affymetrix UK BiLEVE Axiom array on an initial set of ≈50,000 participants; the remaining ≈450,000 participants were genotyped using the Affymetrix UK Biobank Axiom array. The 2 arrays are extremely similar (with over 95% common content). Quality control and imputation [to over 39 million Haplotype Reference Consortium single nucleotide polymorphisms (SNPs) including more than 8 million SNPs with a minor allele frequency >1%] were performed centrally by UK Biobank. IMPUTE2 (*https://mathgen.stats.ox.ac.uk/impute/impute_v2.html#home*) was used for imputation to the Haplotype Reference Consortium v.1.1 panel.

Model used for genetic associations

The recently released version of BOLT-LMM Bayesian mixed model association method (*https://www.biorxiv.org/content/early/2017/09/27/194944*) was used for the associations between imputed SNPs and eBMD (on a BMD T-score scale). This method was developed to produce highly powered, robust test statistics when run on all European samples (retaining related individuals) in the UK Biobank. The model was adjusted for sex, age, and weight. The genome-wide association study of estimated ultrasound BMD using this methodology was recently made available for public download (*https://data.broadinstitute.org/alkesgroup/UKBB/*). For the present study, we used these downloaded data and searched for possible associations specifically between imputed SNPs (minor allele frequency (MAF) >1%) in the *NOTUM* locus ±25 kb from the genes' start/end limits and eBMD. In total, 125 SNPs with a minor allele frequency > 1% were tested, and we applied a conservative Bonferroni correction for these SNPs, setting a value of $P = 0.05/125 = 4.0 \times 10^{-4}$ as a significance threshold.

RESULTS

Heterozygous female *Notum*-inactivated mice have increased cortical bone thickness

To determine the role of NOTUM in the skeleton, we developed a mouse model with global *Notum* inactivation ($Notum^{-/-}$). This model had exons 2–8 of the *Notum* gene deleted ($Notum^{-/-}$; **Fig. 1*A***). A majority of $Notum^{-/-}$ mice (≈90%) died during embryonal development, and the few mice surviving until 13 wk of age were severely growth inhibited. However, heterozygous $Notum^{+/-}$ mice had normal embryonic development and were born apparently healthy and had a normal body weight growth until 13 wk of age (Fig. 1*B*). In addition, $Notum^{+/-}$ mice displayed normal bone length of femur (Fig. 1*C*) and normal weights of several visceral organs (Fig. 1*D*). When comparing the *Notum* expression in different tissues, the highest expression in WT mice was observed for liver and diaphyseal cortical bone (Fig. 1*E*). $Notum^{+/-}$ mice had reduced *Notum* mRNA levels in both liver and bone compared with WT mice (Fig. 1*E*), and no *Notum* expression was observed in the few surviving severely growth-inhibited $Notum^{-/-}$ mice. As expected, the recombination of the *Notum* allele in liver and bone was complete in the $Notum^{-/-}$ mice, and it was ≈50% in these 2 tissues of $Notum^{+/-}$ mice (Fig. 1*F*).

Dual-energy X-ray absorptiometry (DXA) analyses revealed that the total femur BMD was significantly increased in female $Notum^{+/-}$ mice compared with WT mice (Fig. 1*G*), and a similar nonsignificant trend was observed for total body BMD (Fig. 1*H*). We next evaluated the cortical and trabecular bone compartments separately using high-resolution μCT analyses. The femur middiaphyseal cortical bone area (Fig. 1*I*), cortical thickness (Fig. 1*J*), and the estimated bone strength polar moment of inertia (Fig. 1*K*) were significantly increased in female $Notum^{+/-}$ mice compared with WT mice, whereas cortical porosity (Fig. 1*L*) and cortical volumetric BMD (Fig. 1*M*) were unaffected. Three-point bending analyses of the diaphyseal region of the humerus revealed increased cortical bone strength in female $Notum^{+/-}$ mice compared with WT mice (Fig. 1*N*). In contrast, female $Notum^{+/-}$ mice had normal trabecular bone volume/tissue volume (BV/TV) fraction in both the distal metaphyseal region of femur (Fig. 1*O*) and in the L5 vertebral body (Fig. 1*P*). Thus, heterozygous female *Notum*-inactivated mice have specifically increased cortical bone thickness and bone strength. There was no significant bone phenotype in the male $Notum^{+/-}$ mice compared with male WT mice (Supplemental Table S1).

Osteoblast-derived NOTUM is the principal source of NOTUM in bone

Because *Notum* expression was high in cortical bone, we hypothesized that the cortical bone phenotype in the heterozygote female *Notum*-inactivated mice might be caused by lack of *Notum* expression by osteoblast lineage cells in cortical bone. However, a role of other contributing cell types in the bone compartment or by circulating factors such as liver-derived *Notum* or other indirect systemic effects could not be excluded. To determine the source of NOTUM in cortical bone and the function of osteoblast-derived NOTUM *in vivo*, we generated a conditional *Notum*-inactivated mouse model targeting osteoblasts and osteocytes. A mouse model with exons 2–8 of *Notum* flanked by *LoxP* sites ($Notum^{flox/flox}$, **Fig. 2*A***) was used (16). To achieve inactivation of NOTUM early in the osteoblast lineage, we generated *Runx2-creNotum*$^{flox/flox}$ mice, which express Cre recombinase driven by the Runx2 promoter, a promoter that is expressed specifically in early osteoblast lineage cells but not in osteoclasts (Fig. 2*A*) (18). *Runx2-creNotum*$^{flox/flox}$ mice had substantial and specific recombination of the $Notum^{flox}$ allele in bone (Fig. 2*B*), resulting in 98 ± 0.4 and 79 ± 9.5% lower *Notum* mRNA levels in cortical bone of female and male mice, respectively, compared to corresponding $Notum^{flox/flox}$ mice (Fig. 2*C*). Analyses of isolated calvarial cells, containing a large proportion of osteoblasts, showed that cells from *Runx2-creNotum*$^{flox/flox}$ mice had substantially lower levels of *Notum* mRNA expression compared with cells from $Notum^{flox/flox}$ mice (Fig. 2*D*). Expression of *Notum* mRNA in bone marrow macrophages was close to the detection limit and was not affected by osteoblast lineage–specific *Notum* inactivation (Fig. 2*D*). These findings demonstrate that osteoblast lineage–derived NOTUM is the principal source of NOTUM in cortical bone.

Runx2-creNotum$^{flox/flox}$ mice displayed normal embryonic development and were born apparently healthy and had a normal body weight growth through 17 wk of age (Fig. 2*E*). In addition, *Runx2-creNotum*$^{flox/flox}$ mice had normal bone length of femur (Fig. 2*F*) and normal weights of several visceral organs (Fig. 2*G*). DXA analyses revealed that both *male and female Runx2-creNotum*$^{flox/flox}$ mice developed increased total body BMD during sexual maturation (Fig. 2*H*). Total femur BMD was also significantly increased in both adult male and adult female *Runx2-creNotum*$^{flox/flox}$ mice compared with corresponding $Notum^{flox/flox}$ mice (Fig. 2*I*). Thus, osteoblast-derived NOTUM is the principal source of NOTUM in bone and decreases total body BMD.

Osteoblast-derived NOTUM reduces cortical but not trabecular bone mass

Detailed CT analyses of the cortical diaphyseal bone in femur revealed increased cortical bone area (**Fig. 3*A***), cortical bone thickness (Fig. 3*B*), and cortical polar moment of inertia (Fig. 3*C*) in adult *Runx2-creNotum*$^{flox/flox}$ mice compared to control mice. However, neither the cortical porosity (Fig. 3*D*) nor the cortical volumetric BMD (Fig. 3*E*) were affected in the *Runx2-creNotum*$^{flox/flox}$ mice. Furthermore, the cortical thickness and cortical area of vertebral body L5 were increased in female *Runx2-creNotum*$^{flox/flox}$ mice compared to control mice and a similar nonsignificant trend ($P = 0.09$) was observed for the cortical bone area in male mice (Supplemental Table S2). The increased amount of cortical bone resulted in a substantial increase in mechanical strength (maximum load; Fig. 3*F*) and whole-bone work-to-fracture (Fig. 3*G*) of the cortical bone, whereas the structural stiffness (Fig. 3*H*) was not significantly affected when evaluated by using 3-point

bending in the diaphyseal region of the humerus. *Runx2-creNotum*$^{flox/flox}$ male mice had normal BV/TV in both the distal metaphyseal region of femur (Fig. 3*I*) and in the L5 vertebral body (Fig. 3*J*). *Runx2-creNotum*$^{flox/flox}$ female mice had also a normal BV/TV in the distal metaphyseal region of femur (Fig. 3*I*) but a slightly decreased BV/TV in the L5 vertebral body (Fig. 3*J*). The increased cortical thickness but not trabecular bone mass is a phenocopy, although slightly more pronounced, of the heterozygote female global *Notum*-inactivated mice. The increased cortical bone thickness in both the male and the female mice with osteoblast lineage–specific *Notum* inactivation was the result of an increased periosteal circumference (Fig. 3*K*), whereas the endocortical circumference was not reduced (Fig. 3*L*). However, cortical histomorphometric analyses performed at 17 wk of age did not identify any significant effects on bone formation rate or on numbers of osteoblasts or osteoclasts per bone surface (Supplemental Table S3).

Inducible inactivation of *Notum* increases cortical periosteal bone formation

Although very informative, the studies using osteoblast lineage–specific *Notum* inactivation could not separate between developmental effects of NOTUM and its effects on adult bone metabolism. Therefore, to evaluate the effect of *Notum* specifically on adult cortical bone homeostasis and the underlying mechanisms, we developed a mouse model with tamoxifen-inducible *Notum* inactivation in adult mice. To this end, we bred *Notum*$^{flox/flox}$ mice with *CAGGCre-ER* transgenic mice (19) expressing a

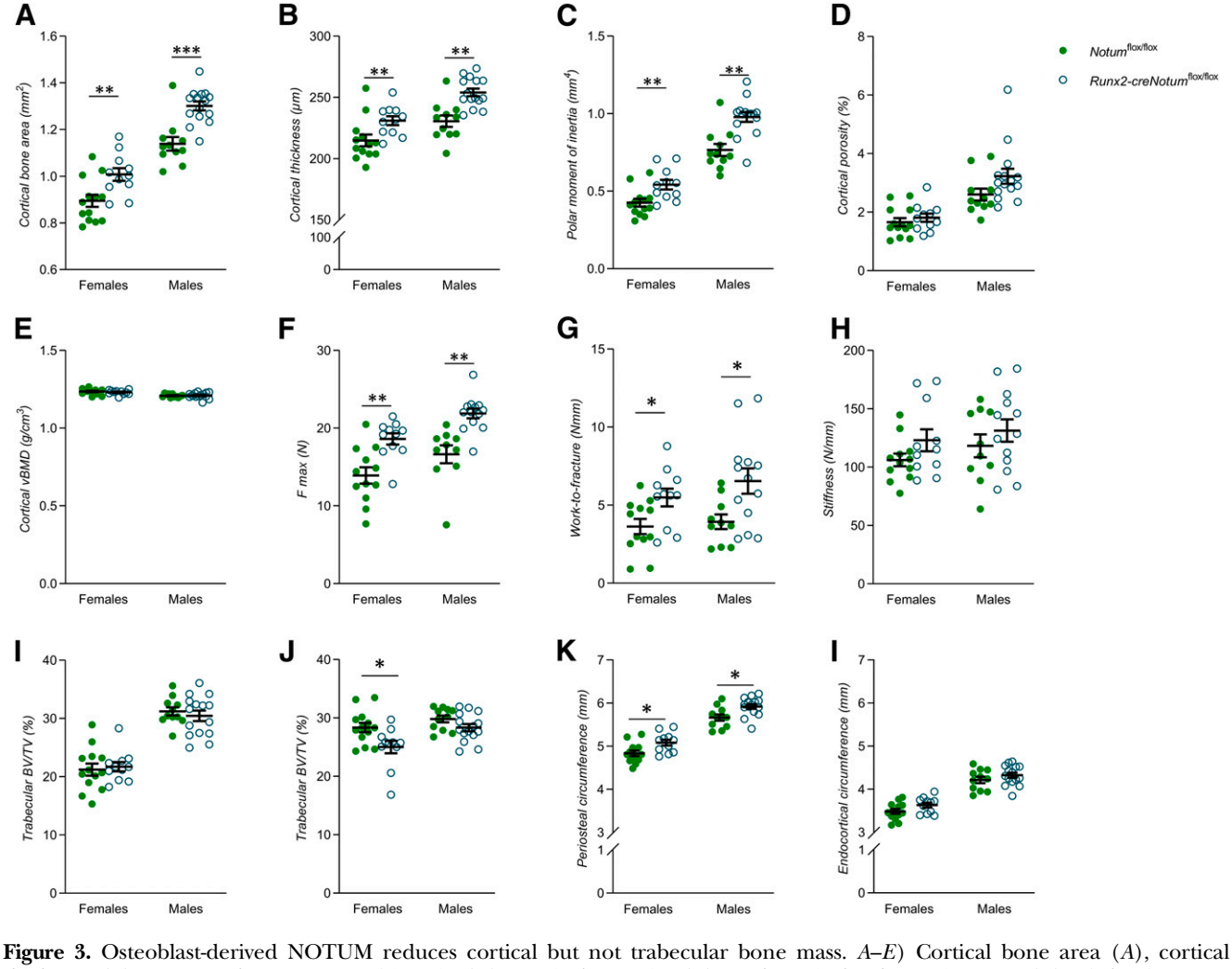

Figure 3. Osteoblast-derived NOTUM reduces cortical but not trabecular bone mass. *A–E*) Cortical bone area (*A*), cortical thickness (*B*), mean polar moment of inertia (*C*), cortical porosity (*D*), and cortical volumetric BMD (*E*) of the femur as measured by μCT in *Runx2-creNotum*$^{flox/flox}$ (female, $n = 11$; males, $n = 15$) and *Notum*$^{flox/flox}$ (females, $n = 13$; males, $n = 11$) mice. *F–H*) Maximal load (F max) (*F*), whole-bone work-to-fracture (*G*), and (*H*) structural stiffness (*H*) of the humerus as measured by 3-point bending in *Runx2-creNotum*$^{flox/flox}$ (female, $n = 11$; males, $n = 15$) and *Notum*$^{flox/flox}$ (females, $n = 13$; males, $n = 11$) mice. All biomechanical data are whole-bone data. *I, J*) Trabecular BV/TV in the femur (*I*) and vertebral body L5 (*J*) in *Runx2-creNotum*$^{flox/flox}$ mice (females, $n = 11$; males, $n = 15$) and *Notum*$^{flox/flox}$ mice (females, $n = 13$; males, $n = 11$). *K, L*) Periosteal (*K*) and endocortical circumference (*L*) of the femur as measured by μCT in *Runx2-creNotum*$^{flox/flox}$ (females, $n = 11$; males, $n = 15$) and *Notum*$^{flox/flox}$ (females, $n = 13$; males, $n = 11$) mice. Unless otherwise stated, the results refer to 17-wk-old mice. All values are given as means ± SEM. $^*P < 0.05$, $^{**}P < 0.01$ *vs.* *Notum*$^{flox/flox}$ mice (Student's *t* test).

tamoxifen-inducible Cre-mediated recombination system (**Fig. 4*A***). We have previously shown that *CAGGCre-ER* mice do not have a skeletal phenotype (32). All mice evaluated were treated with the same tamoxifen regime, using daily intraperitoneal injections during 3 consecutive days and the phenotype of *CAGGCre-ER-Notum*$^{flox/flox}$ and *Notum*$^{flox/flox}$ mice were compared (Fig. 4*A*). The *Notum* mRNA levels in cortical bone were substantially lower (−63 ± 5%; $P < 0.01$) in tamoxifen-treated *CAGGCre-ER-Notum*$^{flox/flox}$ mice compared with tamoxifen-treated *Notum*$^{flox/flox}$ mice, demonstrating efficient *Notum* inactivation (Fig. 4*B*). To determine the skeletal phenotype in the inducible *Notum* knockout mice, 11-wk-old *Notum*$^{flox/flox}$ and *CAGGCre-ER-Notum*$^{flox/flox}$ mice were treated with tamoxifen and the phenotype was evaluated 31 d after the first tamoxifen dose. The inducible inactivation of *Notum* did not affect body weight, weights of liver, gonadal fat, kidney, spleen or uterus, or the lengths of femur or tibia (Supplemental Table S4). Detailed skeletal analyses using DXA and CT revealed that the total femur BMD ($P < 0.05$) and several diaphyseal cortical bone mass parameter (cortical area, cortical thickness, and cortical moment of inertia; $P < 0.05$) but not BV/TV in the metaphyseal region of tibia were significantly increased in tamoxifen-treated *CAGGCre-ER-Notum*$^{flox/flox}$ mice compared with tamoxifen-treated *Notum*$^{flox/flox}$ mice (**Table 1**).

Dynamic cortical histomorphometry was performed to determine if inducible *Notum* inactivation increased cortical bone thickness *via* increased cortical bone formation. Periosteal mineralized surface (+32 ± 4%; $P < 0.01$; Fig. 4C), mineral apposition rate (+65 ± 16%; $P < 0.05$; Fig. 4*D*), and bone formation rate (+113 ± 25%; $P < 0.01$; Fig. 4*E*) were substantially increased in tamoxifen-treated *CAGGCre-ER-Notum*$^{flox/flox}$ mice compared with tamoxifen-treated *Notum*$^{flox/flox}$ mice. In contrast, endocortical bone formation was not significantly affected by inducible *Notum* inactivation (Fig. 4*F–H*). Static histomorphometry revealed that the periosteal number of osteoblasts (+183 ± 68%; $P < 0.05$) and the periosteal surface covered by osteoblasts (+183 ± 66%; $P < 0.05$) were significantly increased by inducible *Notum* inactivation, whereas the number of osteoblasts on the endocortical side was unchanged (**Table 2**). These mechanistic studies using inducible *Notum* inactivation demonstrate that *Notum* deficiency increases bone formation at the periosteal, but not at the endocortical, side of the cortical bone. For further mechanistic studies including analyses of serum bone markers and gene transcripts, *Notum*$^{flox/flox}$ and *CAGGCre-ER-Notum*$^{flox/flox}$ mice were induced with tamoxifen and evaluated 11 d after the first tamoxifen dose. Although serum levels of the bone resorption marker CTX fragments (Fig. 4*I*) and the mRNA levels of the osteoclast-specific transcript *Acp5* in cortical bone (Fig. 4*J*) were reduced, neither the number of periosteal osteoclasts nor the number of endocortical osteoclasts were significantly altered by *Notum* inactivation (Table 2). Thus, inducible *Notum* inactivation does not seem to influence the number of osteoclasts, but we cannot exclude the possibility that an inhibitory effect on osteoclast activity might have contributed to increased cortical bone thickness.

Silencing of NOTUM increases osteoblast differentiation

To determine if osteoblast-derived NOTUM has the capacity to exert local effects on osteoblasts, *Notum* expression was silenced in osteoblasts using the preosteoblast cell line MC3T3-E1. The cells were silenced 1 and 3 d after seeding and treated with osteogenic medium for 7 d, starting 24 h after the second silencing. Expression of *Notum* mRNA was decreased by 82 ± 9% ($P < 0.001$) and 95 ± 2% ($P < 0.05$) after the first and second silencing (**Fig. 5*A***). Analyses of osteoblast differentiation showed that silencing of *Notum* resulted in enhanced mRNA expression of *Alpl* already 24 h after the second silencing (Fig. 5*B*) and an increased ALP staining (Fig. 5*C*) and a 7-fold increase of ALP activity (Fig. 5*D*) at the end of the cultures, indicating that NOTUM is a negative regulator of osteoblastic differentiation. These findings clearly demonstrate that osteoblast-derived NOTUM has the capacity to exert local effects on osteoblast differentiation.

Recombinant NOTUM protein does not affect osteoclast differentiation or activity

Because the NOTUM expression is very low in osteoclasts, we wanted to explore the possibility that paracrine or endocrine NOTUM might exert effects on osteoclasts. To determine if preosteoclasts or osteoclasts have the capacity to respond to NOTUM, we treated BMMs with M-CSF/RANKL in the absence and presence of recombinant human NOTUM. First, we demonstrated that the used recombinant human NOTUM had effective lipase activity (Supplemental Fig. S3). Recombinant human NOTUM did not affect the formation of TRAP-positive multinucleated osteoclasts (Fig. 5*E*) or M-CSF/RANKL-induced expression of the osteoclastic genes *Acp5*, *Ctsk*, and *Nfatc1* (Fig. 5*F–H*), when BMMs were cultured on plastic dishes. Recombinant NOTUM affected neither osteoclast formation on bone disc as assessed by release of TRAP5b (Fig. 5*I*) nor osteoclast resorption activity analyzed by release of CTX (Fig. 5*J*), suggesting that NOTUM does not exert any direct effects on osteoclasts. These data, however, do not exclude the possibility that NOTUM could have indirect effects on osteoclasts *in vivo.*

Large-scale human genetic analyses reveal that the *NOTUM* locus is associated with BMD

To determine if the *NOTUM* locus is also associated with bone mass in humans, we used the complete UK Biobank data set, currently the most powerful available resource for human genetic analyses of a bone phenotype (*https://www.biorxiv.org/content/early/2017/09/27/194944*). We searched for possible associations between imputed SNPs specifically in the *NOTUM* locus (defined as ± 25 kb from the gene start and end limits) and BMD as estimated by

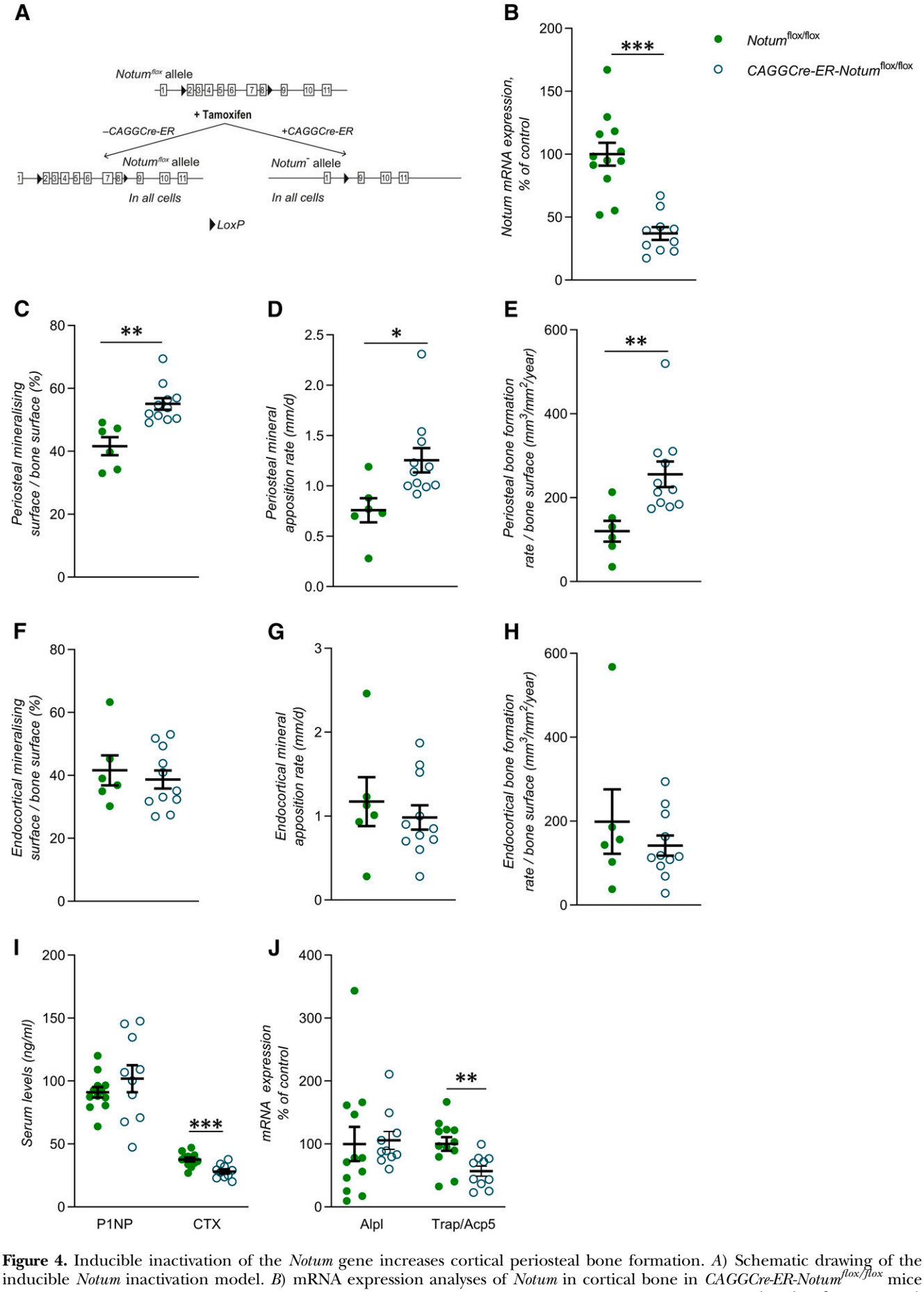

Figure 4. Inducible inactivation of the *Notum* gene increases cortical periosteal bone formation. *A*) Schematic drawing of the inducible *Notum* inactivation model. *B*) mRNA expression analyses of *Notum* in cortical bone in *CAGGCre-ER-Notum*$^{flox/flox}$ mice

(*continued on next page*)

quantitative ultrasound of the heel (eBMD; available in 445,921 European subjects). In total, we tested 125 SNPs with a minor allele of >1% and identified 2 independent genetic signals located upstream of *NOTUM* (**Table 3** and Supplemental Fig. S4*A, B*) both associated with a *P* value of $<10^{-10}$, providing compelling statistical evidence that genetic variation arising from the *NOTUM* locus is associated with eBMD in humans. One of the identified SNPs, rs35344256 (Supplemental Fig. S4*A*; C allele associated with reduced eBMD), is a common variant with minor allele frequency of 31%, whereas the other SNP, rs147901986 (Supplemental Fig. S4*B*; G allele associated with increased eBMD), is a low-frequency variant with minor allele frequency of 2.9% (Table 3).

DISCUSSION

NOTUM is a secreted WNT lipase reducing WNT activity (9, 10). As the role of NOTUM *in vivo* is essentially unknown, we developed global, cell-specific, and inducible *Notum*-inactivated mouse models. We herein demonstrate that osteoblast lineage–derived NOTUM is a crucial determinant specifically of cortical bone mass and strength *via* regulation of periosteal bone formation in mice and that genetic variants in the *NOTUM* locus are robustly associated with BMD in humans.

WNT proteins signal through both the canonical WNT pathway and the noncanonical WNT pathways (1, 2, 14, 33, 34). Activation of canonical β-catenin signaling increases bone mass, and rare human genetic mutations affecting bone have been identified in components of the canonical and noncanonical WNT signaling machinery (1, 4, 35–39). Recent *in vitro* studies demonstrate that NOTUM inactivates WNTs by removing their attached lipid group essential for activation of Frizzled receptors (9, 10). To evaluate if NOTUM may be a local factor in bone, we first developed and characterized a mouse model with global *Notum* inactivation. Because a majority of $Notum^{-/-}$ mice died during embryonal development, it was not possible to determine the physiologic role of NOTUM for any phenotype in adult $Notum^{-/-}$ mice. However, heterozygous Notum-inactivated mice, having significantly reduced *Notum* expression in multiple tissues, were born apparently healthy and displayed a normal body weight and longitudinal bone growth. The female mice with heterozygous global *Notum* inactivation had increased cortical bone thickness and bone strength but normal BV/TV. Although our studies using heterozygous female mice with global *Notum* inactivation indicated that NOTUM reduces cortical but not trabecular bone mass, these studies were difficult to interpret. First, a majority of homozygous *Notum*-inactivated mice died during embryonic development, demonstrating that NOTUM is required for normal development and that it therefore is not possible to use this mouse model to determine the effect of NOTUM on adult bone metabolism. Second, although female mice with global *Notum* inactivation had increased cortical bone thickness, no significant bone phenotype was observed in heterozygous male mice. Finally, the experiments using global *Notum* inactivation could not determine the source of NOTUM with an impact on cortical bone. Because *Notum* expression was high in the cortical bone, we hypothesized that the cortical bone phenotype in the heterozygote female *Notum*-inactivated mice might be caused by lack of *Notum* expression by osteoblast lineage cells in cortical bone. However, a role of other contributing cell types in the bone compartment or by circulating factors, such as liver-derived Notum, or other indirect systemic effects could not be excluded using this mouse model.

To determine if the relatively high *Notum* expression in cortical bone is osteoblast-derived and to determine the *in vivo* role of osteoblast-derived NOTUM, we developed a conditional *Notum*-inactivated mouse model with inactivation of *Notum* in both osteoblasts and osteocytes. Using this model, we clearly demonstrated that osteoblast lineage cells are the principal source of NOTUM in cortical bone, and we next determined the functional role of osteoblast-derived NOTUM. In contrast to homozygous mice with global *Notum* inactivation, those with osteoblast lineage–specific *Notum* inactivation were born healthy and displayed a normal body weight and longitudinal bone growth. These findings demonstrate that the severe developmental effects in the global *Notum*-inactivated homozygous mice are caused by lack of NOTUM in other cells than osteoblast lineage cells. CT analyses, separating the cortical and trabecular bone compartments revealed that both adult male and adult female mice with osteoblast lineage–specific inactivation of *Notum* had increased cortical bone thickness in the long bones, whereas no increase was observed on BV/TV in the

(22-wk-old male mice, $n = 10$) and $Notum^{flox/flox}$ mice ($n = 12$). *C–E*) Mineralizing surface per bone surface (*C*), mineral apposition rate (*D*), and bone formation rate per bone surface (*E*) on the periosteal side of tibia as measured by histomorphometry in *CAGGCre-ER-*$Notum^{flox/flox}$ mice (15-wk-old female mice, $n = 11$) and $Notum^{flox/flox}$ mice ($n = 6$). *F–H*) Mineralizing surface per bone surface (*F*), mineral apposition rate (*G*), and bone formation rate per bone surface (*H*) on the endocortical side of tibia as measured by histomorphometry in *CAGGCre-ER-*$Notum^{flox/flox}$ mice (15-wk-old female mice, $n = 11$) and $Notum^{flox/flox}$ mice ($n = 6$). *I*) Levels of procollagen type I N-terminal propeptide (P1NP, left) and (CTX) fragments (right) measured in serum in *CAGGCre-ER-*$Notum^{flox/flox}$ mice (22-wk-old male mice, $n = 12$) and $Notum^{flox/flox}$ mice ($n = 10$). *J*) mRNA expression analyses of ALP (*Alpl*, left) and TRAP (*Trap/Acp5*, right) in cortical bone of *CAGGCre-ER-*$Notum^{flox/flox}$ mice (22-wk-old male mice, $n = 10$) and $Notum^{flox/flox}$ mice ($n = 12$). All values are given as means ± SEM. $^*P < 0.05$, $^{**}P < 0.01$, $^{***}P < 0.001$ *vs.* $Notum^{flox/flox}$ mice (Student's *t* test).

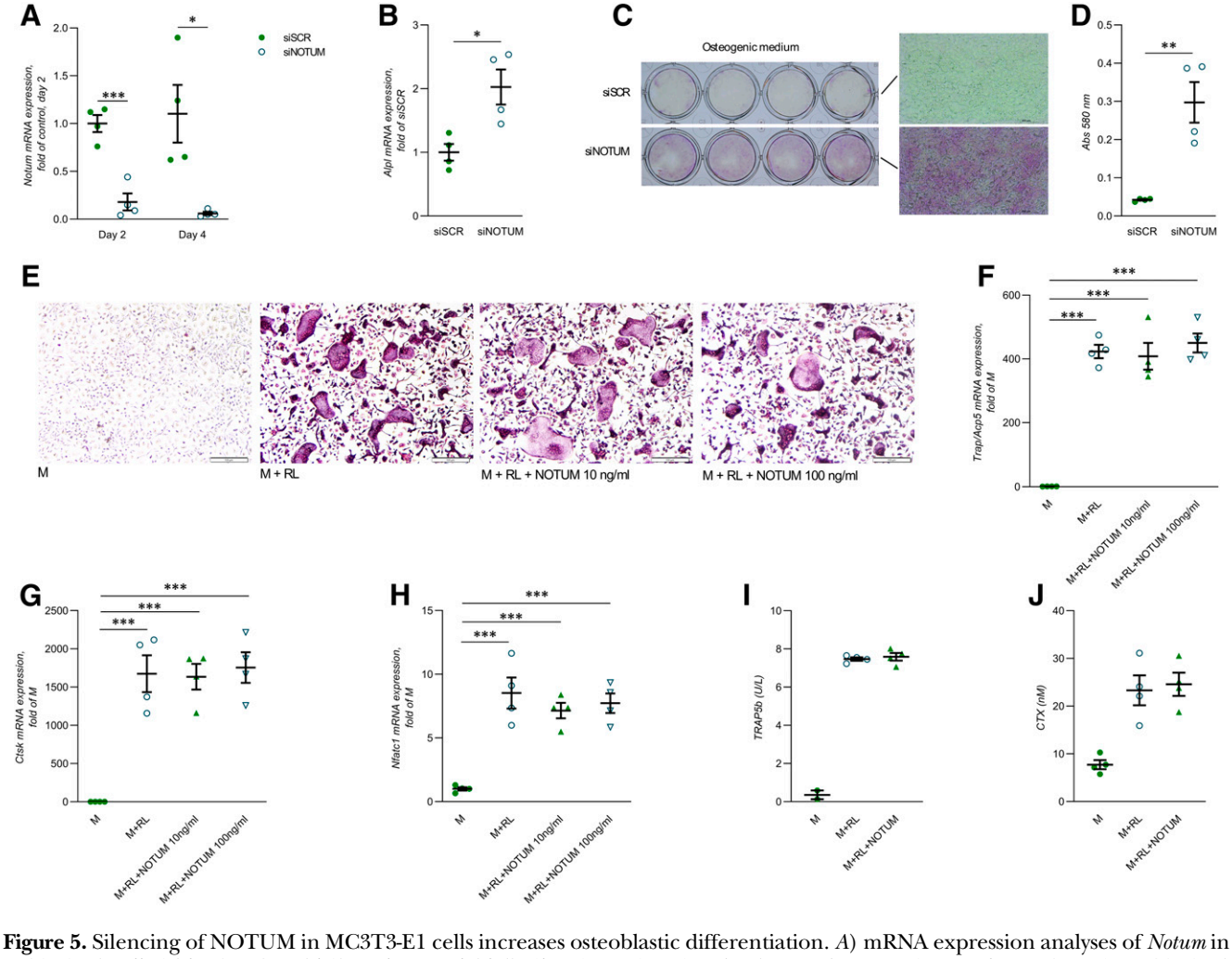

Figure 5. Silencing of NOTUM in MC3T3-E1 cells increases osteoblastic differentiation. *A*) mRNA expression analyses of *Notum* in MC3T3-E1 cells 24 h after first (d 2) and second (d 4) silencing using siRNA. *B*) mRNA expression analyses of *Alpl* in MC3T3-E1 cells 24 h after second silencing of *Notum* using siRNA. *C*) ALP staining of MC3T3-E1 cells after silencing of *Notum* and cultured in osteogenic medium for 7 d. *D*) ALP enzymatic activity in MC3T3-E1 cells after silencing of *Notum* and cultured in osteogenic medium for 7 d. *E*) TRAP staining of osteoclasts cultured in the presence or absence of recombinant NOTUM protein for 3 d. *F–H*) Expression of *Acp5* (*F*), *Ctsk* (*G*), and *Nfatc1* (*H*) in osteoclasts cultured in the presence or absence of recombinant NOTUM for 3 d. *I*) TRAP5b protein released into osteoclast culture media during d 7–10 of culture on bone discs in the presence or absence of recombinant NOTUM. *J*) CTX released into osteoclast culture medium during d 7–10 of culture on bone discs in the presence or absence of recombinant NOTUM. M, M-CSF; RL, RANKL; siSCR, control scramble siRNA; siNOTUM, NOTUM-specific siRNA. All values are given as means ± SEM. $^*P < 0.05$, $^{**}P < 0.01$, $^{***}P < 0.001$ *vs.* siSCR [Student's *t* test (*A*, *B*, *D*)]; $^{***}P < 0.001$ *vs.* the M treatment [1-way ANOVA and Tukey's multiple comparison test (*F–H*)]; $n = 4$ wells/treatment. All cell culture experiments were repeated at least twice with similar results.

vertebrae or in the long bones. Although slightly more pronounced, this specific cortical bone phenotype in mice with osteoblast lineage–specific *Notum* inactivation is very similar to the cortical bone phenotype observed in the female mice with heterozygous global Notum inactivation, supporting the concept that osteoblast-derived NOTUM is mediating the effects on cortical bone thickness.

Three-point bending analyses revealed substantially increased whole-bone mechanical bone strength in mice with osteoblast lineage–specific inactivation of *Notum* compared with control mice, demonstrating that the increased cortical bone thickness resulted in increased bone strength. It is a limitation with the present study that the cortical bone quality was only evaluated by cortical porosity measurements, whereas no analyses of the tissue material properties were performed, precluding statements on the cortical bone quality. Another limitation with the present study is that the cortical tissue organization estimated by informative collagen type I orientation analyses was not performed (40–42). The increased cortical bone thickness in both the male and the female mice with osteoblast lineage–specific *Notum* inactivation was the result of an increased periosteal circumference, whereas the endocortical circumference was not reduced, suggesting that the increased cortical bone thickness was caused by cortical periosteal bone formation. However, the lack of significant effects on cortical bone formation rates and number of osteoclasts in 17-wk-old adult mice with lifelong osteoblast lineage–specific *Notum*

TABLE 3. *Genetic variants in the NOTUM locus are associated with BMD*

SNP	Chr	Position	A1	A2	AF	β	SE	P	N
rs35344256	17	79934194	C	A	0.69	−0.0134	0.0020	1.5E−11	445921
rs147901986	17	79921522	G	A	0.97	0.0386	0.0059	4.6E−11	445921

Large-scale human genetic analyses revealed that genetic variants in the *NOTUM* locus are associated with BMD. We specifically searched for possible associations between imputed SNPs (minor allele frequency >1%) in the *NOTUM* locus ±25 kb (in total 125 SNPs with a minor allele frequency >1% were evaluated) and BMD as estimated by quantitative ultrasound of the heel. A1, effect allele; A2, other allele; AF, allele frequency of allele 1. Independent SNPs associated with BMD and with $P < 1 \times 10^{-10}$. β given as SD change in eBMD per effect allele.

inactivation indicated that the increased cortical bone thickness of these mice was a result of effects occurring earlier in life. Therefore, to evaluate the effect of NOTUM on adult cortical bone homeostasis and the underlying mechanisms, we developed a mouse model with tamoxifen-inducible *Notum* inactivation in adult mice. An increase specifically of cortical bone mass was observed only 4 wk after the inducible *Notum* inactivation in adult mice, excluding confounding developmental effects and demonstrating that endogenous NOTUM exerts crucial effects on cortical bone homeostasis in adult mice. The mechanistic studies using the mouse model with inducible inactivation of *Notum* revealed that NOTUM deficiency increases periosteal bone formation as a result of a combination of increased periosteal mineralized surface, reflecting the number of active osteoblasts, and increased periosteal mineral apposition rate, reflecting the activity of osteoblasts. An effect on cortical periosteal bone formation was further supported by the observed increased number of osteoblasts on the periosteal surface in mice with inducible *Notum* inactivation. Collectively, the acute mechanistic data, using inducible *Notum* inactivation, demonstrate that the increased periosteal cortical circumference, observed in mice with lifelong chronic osteoblast lineage–specific inactivation of *Notum*, is primarily caused by increased periosteal bone formation.

A local effect of osteoblast-derived *Notum* on osteoblasts is supported by our finding that *Notum* silencing enhanced osteoblast differentiation in cultured MC3T3-E1 osteoblasts. In contrast, very low *Notum* expression was observed in osteoclast cultures and recombinant human NOTUM did not exert any significant direct effect on osteoclast formation or activity *in vitro*. Although serum levels of the bone resorption marker CTX and the mRNA levels of the osteoclast-specific transcript *Acp5* in cortical bone were reduced by inducible *Notum* inactivation, we were unable to detect any decrease of the number of osteoclasts in cortical bone. Thus, NOTUM does not seem to exert any effect on osteoclastogenesis in cortical bone. Our findings overall demonstrate that the principal mechanism for the increased cortical bone thickness in *Notum*-inactivated mice is an increased periosteal bone formation *via* depletion of local inhibitory effects of osteoblast-derived NOTUM on osteoblast number and activity.

Very similar increases on cortical bone thickness and cortical bone strength were observed in male and female mice for the mouse model with osteoblast lineage–specific *Notum* inactivation. In contrast, for the mouse model with heterozygous global *Notum* inactivation, a significant cortical bone phenotype was only observed in female mice, suggesting that female mice might be more sensitive to changes in *Notum* expression. It is a limitation with the present study that possible sex differences in the effect on cortical bone thickness were not investigated in the inducible *Notum*-inactivated mouse model.

Cortical bone mass is a major determinant of bone strength and therefore of susceptibility to fractures (3, 43). With aging, the mass of cortical bone may decrease more than the mass of trabecular bone, and fractures occurring in older persons result to a large extent from cortical bone fragility (43, 44). Although progress has been made in therapeutic approaches to reduce the risk of vertebral fracture (which occurs at sites rich in trabecular bone), currently available treatments do little to reduce the risk of nonvertebral fracture, which results mostly from cortical bone fragility (4, 43, 45, 46). Thus, there is a medical need to improve the therapy for nonvertebral fractures, and our present finding that osteoblast-derived *Notum* reduces cortical bone mass suggests that methods inhibiting the effect of NOTUM might increase cortical bone mass and thereby reduce nonvertebral fracture risk.

Mice with osteoblast- or osteocyte-specific inactivation of *Wntless* (*Wls*, previously known as Gpr177), which is required for the secretion of WNT ligands from cells, have substantially reduced bone mass, illustrating the crucial role of osteoblast lineage–derived WNTs for bone homeostasis (47). In contrast to mice with osteoblast lineage–specific *Wls* inactivation (displaying a marked reduction of both trabecular and cortical bone mass) (47), osteoblast lineage–specific *Notum* inactivation resulted specifically in increased cortical bone thickness without affecting trabecular bone mass. Combined, these findings suggest that NOTUM mainly renders WNTs inactive in cortical bone, and this notion is supported by our observation that the *Notum* expression is higher in cortical than in trabecular bone. The fact that patients with Pyle's disease, caused by recessive mutation in the *SFRP4* gene, encoding a soluble WNT inhibitor, have thin cortical but dense trabecular bone, further demonstrates that WNTs and WNT modulators exert site-specific effects in the skeleton (46).

Previous studies have demonstrated that osteoblast-derived WNT16 increases cortical but not trabecular bone mass, and it is therefore possible that osteoblast-derived WNT16 is inactivated by osteoblast-derived NOTUM in cortical bone (2, 48). We recently observed that inducible

Wnt16 inactivation in adult mice reduces periosteal cortical bone formation (32). In addition, we herein demonstrate that inducible inactivation of the WNT lipase *Notum* in adult mice increases periosteal cortical bone formation, suggesting that there may be a local periosteal interaction between WNT16 and NOTUM for the regulation of bone formation. We propose that in adult mice, WNT16-mediated periosteal bone formation might be inhibited by a local NOTUM-mediated negative feedback. A role of intact palmitoleoylation of WNTs for periosteal bone growth is supported by our recent finding that inhibition of Porcupine, the enzyme responsible for palmitoleoylation of WNTs, reduces periosteal but not endocortical bone formation (49). The trabecular bone phenotype in mice with osteoblast lineage–specific inactivation of *Wls* most likely is mediated by loss of WNTs not inactivated by NOTUM within the trabecular bone microenvironment (47). Collectively, these findings demonstrate that WNTs may exert compartment-specific effects on bone homeostasis and that NOTUM most likely inactivates WNTs with a crucial effect specifically on cortical bone.

It has recently been reported that substances inhibiting the lipase activity of NOTUM increased cortical bone thickness (13, 50, 51). These substances, selected based on their capacity to inhibit lipase activity and canonical signaling specifically by WNT3A, increased cortical bone thickness mainly *via* an increased endocortical bone formation, whereas inactivation of endogenous NOTUM in the present study increased cortical bone thickness mainly *via* increased periosteal bone formation. This difference in the predominant cortical bone surface involved might be caused by differences in the effects of inactivation of endogenous NOTUM and the effects of pharmacological inhibition of lipase activity, resulting in enhanced WNT3A-mediated canonical signaling. First, endogenous NOTUM may exert lipase independent effects; second, the lipase substrate specificity, both regarding WNTs known to control cortical bone homeostasis such as WNT16 and other non-WNT proteins, may differ between endogenous NOTUM and the pharmacological effect of the developed substances.

Finally, we evaluated if the *NOTUM* locus is associated with bone mass also in humans. To this end, we used the recently released complete UK Biobank data set (n = 445,921 European subjects) to test genetic variation in the *NOTUM* locus for association with eBMD variation in the most powered setting available. We identified 2 independent genetic variants in the *NOTUM* locus that are associated with eBMD. This finding is the first indication that the *NOTUM* locus is involved in the regulation of bone mass also in humans. Subsequent studies assessing whether these genetic variants in the *NOTUM* locus are specifically associated with cortical bone thickness are warranted in deeper phenotyped cohorts assessed by computer tomography.

In summary, we demonstrate that osteoblast-derived NOTUM is an essential regulator of cortical bone mass *via* effects on periosteal bone formation in adult mice and that genetic variation in the *NOTUM* locus is associated with BMD in humans. Therapies targeting osteoblast-derived NOTUM may constitute useful and specific treatments to reduce the risk of nonvertebral fractures. FJ

ACKNOWLEDGMENTS

The authors thank Lotta Uggla, Biljana Aleksic, Anna Westerlund, and Anette Hansevi (all from the University of Gothenburg) for excellent technical assistance, and Carolina Medina-Gomez (Erasmus University Rotterdam) for support in the human genetic analyses. This study was supported by the Swedish Research Council, the Swedish Foundation for Strategic Research, the Swedish state under the agreement between the Swedish government and the county councils, the ALF-agreement in Gothenburg (Grants 238261, 226481, and 237551), the IngaBritt and Arne Lundberg Foundation, the Royal 80 Year Fund of King Gustav V, the Torsten and Ragnar Söderberg's Foundation, the Knut and Alice Wallenberg Foundation, the Novo Nordisk Foundation, and São Paulo Research Foundation (Grant 2014/05283-3). J.T. was supported by the Deutsche Forschungsgemeinschaft (DFG) Collaborative Research Centre (CRC) 1149, and G.C.N. was supported by Coordenação de Aperfeiçoamento de Pessoal de Nível Superior (CAPES; Finance Code 001). S.M.-S. and K.H.N. share first authorship. The authors declare no conflicts of interest.

AUTHOR CONTRIBUTIONS

S. Movérare-Skrtic and K. H. Nilsson were responsible for the animal experiments; P. Henning and T. Funck-Brentano assisted with animal experiments; M. Nethander, F. Rivadeneira, and C. Ohlsson performed the human genetic analyses; A. Koskela and J. Tuukkanen performed the 3-point bending experiments; G. Coletto Nunes and P. P. C. Souza performed studies using MC3T3-E1 osteoblasts; P. Henning and U. H. Lerner were responsible for primary cell cultures of osteoblasts and osteoclasts; J. Tuckermann provided the *Runx2-cre* mice; C. Perret provided the *Notum*^{flox} mice; S. Movérare-Skrtic, U. H. Lerner, and C. Ohlsson designed and supervised the project; and S. Movérare-Skrtic, K. H. Nilsson, U. H. Lerner, and C. Ohlsson wrote the manuscript.

REFERENCES

1. Lerner, U. H., and Ohlsson, C. (2015) The WNT system: background and its role in bone. *J. Intern. Med.* **277**, 630–649
2. Movérare-Skrtic, S., Henning, P., Liu, X., Nagano, K., Saito, H., Börjesson, A. E., Sjögren, K., Windahl, S. H., Farman, H., Kindlund, B., Engdahl, C., Koskela, A., Zhang, F. P., Eriksson, E. E., Zaman, F., Hammarstedt, A., Isaksson, H., Bally, M., Kassem, A., Lindholm, C., Sandberg, O., Aspenberg, P., Sävendahl, L., Feng, J. Q., Tuckermann, J., Tuukkanen, J., Poutanen, M., Baron, R., Lerner, U. H., Gori, F., and Ohlsson, C. (2014) Osteoblast-derived WNT16 represses osteoclastogenesis and prevents cortical bone fragility fractures. *Nat. Med.* **20**, 1279–1288
3. Ohlsson, C., Sundh, D., Wallerek, A., Nilsson, M., Karlsson, M., Johansson, H., Mellström, D., and Lorentzon, M. (2017) Cortical bone area predicts incident fractures independently of areal bone mineral density in older men. *J. Clin. Endocrinol. Metab.* **102**, 516–524
4. Baron, R., and Hesse, E. (2012) Update on bone anabolics in osteoporosis treatment: rationale, current status, and perspectives. *J. Clin. Endocrinol. Metab.* **97**, 311–325
5. Ohlsson, C., Bengtsson, B. A., Isaksson, O. G., Andreassen, T. T., and Slootweg, M. C. (1998) Growth hormone and bone. *Endocr. Rev.* **19**, 55–79
6. Mohan, S., Richman, C., Guo, R., Amaar, Y., Donahue, L. R., Wergedal, J., and Baylink, D. J. (2003) Insulin-like growth factor regulates peak bone mineral density in mice by both growth

hormone-dependent and -independent mechanisms. *Endocrinology* **144**, 929–936
7. Sjögren, K., Liu, J. L., Blad, K., Skrtic, S., Vidal, O., Wallenius, V., LeRoith, D., Törnell, J., Isaksson, O. G., Jansson, J. O., and Ohlsson, C. (1999) Liver-derived insulin-like growth factor I (IGF-I) is the principal source of IGF-I in blood but is not required for postnatal body growth in mice. *Proc. Natl. Acad. Sci. USA* **96**, 7088–7092
8. Bonnet, N., Garnero, P., and Ferrari, S. (2016) Periostin action in bone. *Mol. Cell. Endocrinol.* **432**, 75–82
9. Nusse, R. (2015) Cell signalling: disarming Wnt. *Nature* **519**, 163–164
10. Kakugawa, S., Langton, P. F., Zebisch, M., Howell, S., Chang, T. H., Liu, Y., Feizi, T., Bineva, G., O'Reilly, N., Snijders, A. P., Jones, E. Y., and Vincent, J. P. (2015) Notum deacylates Wnt proteins to suppress signalling activity. *Nature* **519**, 187–192
11. Madan, B., Ke, Z., Lei, Z. D., Oliver, F. A., Oshima, M., Lee, M. A., Rozen, S., and Virshup, D. M. (2016) NOTUM is a potential pharmacodynamic biomarker of Wnt pathway inhibition. *Oncotarget* **7**, 12386–12392
12. Vogel, P., Read, R. W., Hansen, G. M., Powell, D. R., Kantaputra, P. N., Zambrowicz, B., and Brommage, R. (2016) Dentin dysplasia in Notum knockout mice. *Vet. Pathol.* **53**, 853–862
13. Brommage, R., Liu, J., Vogel, P., Mseeh, F., Thompson, A. Y., Potter, D. G., Shadoan, M. K., Hansen, G. M., Jeter-Jones, S., Cui, J., Bright, D., Bardenhagen, J. P., Doree, D. D., Movérare-Skrtic, S., Nilsson, K. H., Henning, P., Lerner, U. H., Ohlsson, C., Sands, A. T., Tarver, J. E., Powell, D. R., Zambrowicz, B., and Liu, Q. (2019) NOTUM inhibition increases endocortical bone formation and bone strength. *Bone Res.* **7**, 2
14. Baron, R., and Kneissel, M. (2013) WNT signaling in bone homeostasis and disease: from human mutations to treatments. *Nat. Med.* **19**, 179–192
15. Cosman, F., Crittenden, D. B., Adachi, J. D., Binkley, N., Czerwinski, E., Ferrari, S., Hofbauer, L. C., Lau, E., Lewiecki, E. M., Miyauchi, A., Zerbini, C. A., Milmont, C. E., Chen, L., Maddox, J., Meisner, P. D., Libanati, C., and Grauer, A. (2016) Romosozumab treatment in postmenopausal women with osteoporosis. *N. Engl. J. Med.* **375**, 1532–1543
16. Canal, F., Charawi, S., Grimber, G., Houbron, C., Drouet, V., Colnot, S., Terris, B., Cavard, C., and Perret, C. (2016) Generation of mice with hepatocyte-specific conditional deletion of Notum. *PLoS One* **11**, e0150997
17. Lallemand, Y., Luria, V., Haffner-Krausz, R., and Lonai, P. (1998) Maternally expressed PGK-Cre transgene as a tool for early and uniform activation of the Cre site-specific recombinase. *Transgenic Res.* **7**, 105–112
18. Rauch, A., Seitz, S., Baschant, U., Schilling, A. F., Illing, A., Stride, B., Kirilov, M., Mandic, V., Takacz, A., Schmidt-Ullrich, R., Ostermay, S., Schinke, T., Spanbroek, R., Zaiss, M. M., Angel, P. E., Lerner, U. H., David, J. P., Reichardt, H. M., Amling, M., Schütz, G., and Tuckermann, J. P. (2010) Glucocorticoids suppress bone formation by attenuating osteoblast differentiation via the monomeric glucocorticoid receptor. *Cell Metab.* **11**, 517–531
19. Hayashi, S., and McMahon, A. P. (2002) Efficient recombination in diverse tissues by a tamoxifen-inducible form of Cre: a tool for temporally regulated gene activation/inactivation in the mouse. *Dev. Biol.* **244**, 305–318
20. Quarta, C., Clemmensen, C., Zhu, Z., Yang, B., Joseph, S. S., Lutter, D., Yi, C. X., Graf, E., García-Cáceres, C., Legutko, B., Fischer, K., Brommage, R., Zizzari, P., Franklin, B. S., Krueger, M., Koch, M., Vettorazzi, S., Li, P., Hofmann, S. M., Bakhti, M., Bastidas-Ponce, A., Lickert, H., Strom, T. M., Gailus-Durner, V., Bechmann, I., Perez-Tilve, D., Tuckermann, J., Hrabě de Angelis, M., Sandoval, D., Cota, D., Latz, E., Seeley, R. J., Müller, T. D., DiMarchi, R. D., Finan, B., and Tschöp, M. H. (2017) Molecular integration of incretin and glucocorticoid action reverses immunometabolic dysfunction and obesity. *Cell Metab.* **26**, 620–632.e6
21. Windahl, S. H., Vidal, O., Andersson, G., Gustafsson, J. A., and Ohlsson, C. (1999) Increased cortical bone mineral content but unchanged trabecular bone mineral density in female ERbeta(-/-) mice. *J. Clin. Invest.* **104**, 895–901
22. Vidal, O., Lindberg, M. K., Hollberg, K., Baylink, D. J., Andersson, G., Lubahn, D. B., Mohan, S., Gustafsson, J. A., and Ohlsson, C. (2000) Estrogen receptor specificity in the regulation of skeletal growth and maturation in male mice. *Proc. Natl. Acad. Sci. USA* **97**, 5474–5479
23. Peng, Z., Li, X., Mäkelä, S., Väänänen, H. K., and Poutanen, M. (2004) Skeletal changes in transgenic male mice expressing human cytochrome p450 aromatase. *J. Bone Miner. Res.* **19**, 1320–1328
24. Shen, Z., Peng, Z., Sun, Y., Väänänen, H. K., and Poutanen, M. (2008) Overexpression of human hydroxysteroid (17beta) dehydrogenase 2 induces disturbance in skeletal development in young male mice. *J. Bone Miner. Res.* **23**, 1217–1226
25. Dempster, D. W., Compston, J. E., Drezner, M. K., Glorieux, F. H., Kanis, J. A., Malluche, H., Meunier, P. J., Ott, S. M., Recker, R. R., and Parfitt, A. M. (2013) Standardized nomenclature, symbols, and units for bone histomorphometry: a 2012 update of the report of the ASBMR Histomorphometry Nomenclature Committee. *J. Bone Miner. Res.* **28**, 2–17
26. Granholm, S., Henning, P., Lindholm, C., and Lerner, U. H. (2013) Osteoclast progenitor cells present in significant amounts in mouse calvarial osteoblast isolations and osteoclastogenesis increased by BMP-2. *Bone* **52**, 83–92
27. Bakker, A. D., and Klein-Nulend, J. (2012) Osteoblast isolation from murine calvaria and long bones. *Methods Mol. Biol.* **816**, 19–29
28. Takeshita, S., Kaji, K., and Kudo, A. (2000) Identification and characterization of the new osteoclast progenitor with macrophage phenotypes being able to differentiate into mature osteoclasts. *J. Bone Miner. Res.* **15**, 1477–1488
29. Granholm, S., Lundberg, P., and Lerner, U. H. (2007) Calcitonin inhibits osteoclast formation in mouse haematopoetic cells independently of transcriptional regulation by receptor activator of NF-kappaB and c-Fms. *J. Endocrinol.* **195**, 415–427
30. Bauer, D. C., Glüer, C. C., Cauley, J. A., Vogt, T. M., Ensrud, K. E., Genant, H. K., and Black, D. M.; Study of Osteoporotic Fractures Research Group. (1997) Broadband ultrasound attenuation predicts fractures strongly and independently of densitometry in older women. A prospective study. *Arch. Intern. Med.* **157**, 629–634
31. Kemp, J. P., Morris, J. A., Medina-Gomez, C., Forgetta, V., Warrington, N. M., Youlten, S. E., Zheng, J., Gregson, C. L., Grundberg, E., Trajanoska, K., Logan, J. G., Pollard, A. S., Sparkes, P. C., Ghirardello, E. J., Allen, R., Leitch, V. D., Butterfield, N. C., Komla-Ebri, D., Adoum, A. T., Curry, K. F., White, J. K., Kussy, F., Greenlaw, K. M., Xu, C., Harvey, N. C., Cooper, C., Adams, D. J., Greenwood, C. M. T., Maurano, M. T., Kaptoge, S., Rivadeneira, F., Tobias, J. H., Croucher, P. I., Ackert-Bicknell, C. L., Bassett, J. H. D., Williams, G. R., Richards, J. B., and Evans, D. M. (2017) Identification of 153 new loci associated with heel bone mineral density and functional involvement of GPC6 in osteoporosis. *Nat. Genet.* **49**, 1468–1475
32. Ohlsson, C., Henning, P., Nilsson, K. H., Wu, J., Gustafsson, K. L., Sjögren, K., Törnqvist, A., Koskela, A., Zhang, F. P., Lagerquist, M. K., Poutanen, M., Tuukkanen, J., Lerner, U. H., and Movérare-Skrtic, S. (2018) Inducible *Wnt16* inactivation: WNT16 regulates cortical bone thickness in adult mice. *J. Endocrinol.* **237**, 113–122
33. Jenny, A. (2010) Planar cell polarity signaling in the Drosophila eye. *Curr. Top. Dev. Biol.* **93**, 189–227
34. Kohn, A. D., and Moon, R. T. (2005) Wnt and calcium signaling: beta-catenin-independent pathways. *Cell Calcium* **38**, 439–446
35. Balemans, W., Patel, N., Ebeling, M., Van Hul, E., Wuyts, W., Lacza, C., Dioszegi, M., Dikkers, F. G., Hildering, P., Willems, P. J., Verheij, J. B., Lindpaintner, K., Vickery, B., Foernzler, D., and Van Hul, W. (2002) Identification of a 52 kb deletion downstream of the SOST gene in patients with van Buchem disease. *J. Med. Genet.* **39**, 91–97
36. Boyden, L. M., Mao, J., Belsky, J., Mitzner, L., Farhi, A., Mitnick, M. A., Wu, D., Insogna, K., and Lifton, R. P. (2002) High bone density due to a mutation in LDL-receptor-related protein 5. *N. Engl. J. Med.* **346**, 1513–1521
37. Brunkow, M. E., Gardner, J. C., Van Ness, J., Paeper, B. W., Kovacevich, B. R., Proll, S., Skonier, J. E., Zhao, L., Sabo, P. J., Fu, Y., Alisch, R. S., Gillett, L., Colbert, T., Tacconi, P., Galas, D., Hamersma, H., Beighton, P., and Mulligan, J. (2001) Bone dysplasia sclerosteosis results from loss of the SOST gene product, a novel cystine knot-containing protein. *Am. J. Hum. Genet.* **68**, 577–589
38. Gong, Y., Slee, R. B., Fukai, N., Rawadi, G., Roman-Roman, S., Reginato, A. M., Wang, H., Cundy, T., Glorieux, F. H., Lev, D., Zacharin, M., Oexle, K., Marcelino, J., Suwairi, W., Heeger, S., Sabatakos, G., Apte, S., Adkins, W. N., Allgrove, J., Arslan-Kirchner, M., Batch, J. A., Beighton, P., Black, G. C., Boles, R. G., Boon, L. M., Borrone, C., Brunner, H. G., Carle, G. F., Dallapiccola, B., De Paepe, A., Floege, B., Halfhide, M. L., Hall, B., Hennekam, R. C., Hirose, T., Jans, A., Jüppner, H., Kim, C. A., Keppler-Noreuil, K., Kohlschuetter, A., LaCombe, D., Lambert, M., Lemyre, E., Letteboer, T., Peltonen, L., Ramesar, R. S., Romanengo, M., Somer, H., Steichen-Gersdorf, E., Steinmann, B., Sullivan, B., Superti-Furga, A., Swoboda, W., van den Boogaard, M. J., Van Hul, W., Vikkula, M., Votruba, M., Zabel, B., Garcia, T., Baron, R., Olsen, B. R., and Warman, M. L.; Osteoporosis-Pseudoglioma Syndrome Collaborative Group. (2001) LDL receptor-related protein 5 (LRP5) affects bone accrual and eye development. *Cell* **107**, 513–523

39. Little, R. D., Recker, R. R., and Johnson, M. L. (2002) High bone density due to a mutation in LDL-receptor-related protein 5. *N. Engl. J. Med.* **347**, 943–944, author reply 943–944
40. Ascenzi, M. G., Chin, J., Lappe, J., and Recker, R. (2016) Non-osteoporotic women with low-trauma fracture present altered birefringence in cortical bone. *Bone* **84**, 104–112
41. Ascenzi, M. G., Lutz, A., Du, X., Klimecky, L., Kawas, N., Hourany, T., Jahng, J., Chin, J., Tintut, Y., Nackenhors, U., and Keyak, J. (2014) Hyperlipidemia affects multiscale structure and strength of murine femur. *J. Biomech.* **47**, 2436–2443
42. Ascenzi, M.-G., Kawas, N. P., Lutz, A., Kardas, D., Nackenhorst, U., and Keyak, J. H. (2013) Individual-specific multi-scale finite element simulation of cortical bone of human proximal femur. *J. Comput. Phys.* **244**, 298–311
43. Zebaze, R. M., Ghasem-Zadeh, A., Bohte, A., Iuliano-Burns, S., Mirams, M., Price, R. I., Mackie, E. J., and Seeman, E. (2010) Intracortical remodelling and porosity in the distal radius and post-mortem femurs of women: a cross-sectional study. *Lancet* **375**, 1729–1736
44. Gori, F., Lerner, U., Ohlsson, C., and Baron, R. (2015) A new WNT on the bone: WNT16, cortical bone thickness, porosity and fractures. *Bonekey Rep.* **4**, 669
45. Black, D. M., and Rosen, C. J. (2016) Postmenopausal osteoporosis. *N. Engl. J. Med.* **374**, 2096–2097
46. Kiper, P. O. S., Saito, H., Gori, F., Unger, S., Hesse, E., Yamana, K., Kiviranta, R., Solban, N., Liu, J., Brommage, R., Boduroglu, K., Bonafé, L., Campos-Xavier, B., Dikoglu, E., Eastell, R., Gossiel, F., Harshman, K., Nishimura, G., Girisha, K. M., Stevenson, B. J., Takita, H., Rivolta, C., Superti-Furga, A., and Baron, R. (2016) Cortical-bone fragility–insights from sFRP4 deficiency in Pyle's disease. *N. Engl. J. Med.* **374**, 2553–2562
47. Zhong, Z., Zylstra-Diegel, C. R., Schumacher, C. A., Baker, J. J., Carpenter, A. C., Rao, S., Yao, W., Guan, M., Helms, J. A., Lane, N. E., Lang, R. A., and Williams, B. O. (2012) Wntless functions in mature osteoblasts to regulate bone mass. *Proc. Natl. Acad. Sci. USA* **109**, E2197–E2204
48. Wergedal, J. E., Kesavan, C., Brommage, R., Das, S., and Mohan, S. (2015) Role of WNT16 in the regulation of periosteal bone formation in female mice. *Endocrinology* **156**, 1023–1032
49. Funck-Brentano, T., Nilsson, K. H., Brommage, R., Henning, P., Lerner, U. H., Koskela, A., Tuukkanen, J., Cohen-Solal, M., Movérare-Skrtic, S., and Ohlsson, C. (2018) Porcupine inhibitors impair trabecular and cortical bone mass and strength in mice. *J. Endocrinol.* **238**, 13–23
50. Han, Q., Pabba, P. K., Barbosa, J., Mabon, R., Healy, J. P., Gardyan, M. W., Terranova, K. M., Brommage, R., Thompson, A. Y., Schmidt, J. M., Wilson, A. G., Xu, X., Tarver, J. E., Jr., and Carson, K. G. (2016) 4H-Thieno[3,2-c]chromene based inhibitors of Notum Pectinacetylesterase. *Bioorg. Med. Chem. Lett.* **26**, 1184–1187
51. Tarver, J. E., Jr., Pabba, P. K., Barbosa, J., Han, Q., Gardyan, M. W., Brommage, R., Thompson, A. Y., Schmidt, J. M., Wilson, A. G. E., He, W., Lombardo, V. K., and Carson, K. G. (2016) Stimulation of cortical bone formation with thienopyrimidine based inhibitors of Notum Pectinacetylesterase. *Bioorg. Med. Chem. Lett.* **26**, 1525–1528

Received for publication March 19, 2019.
Accepted for publication June 17, 2019.